

Electronic excited states of benzene in interaction with water clusters : influence of structure and size

Time dependent density functional theory *vs* multireference wavefunction approaches.

Nadia Ben Amor · Eric Michoulier ·
Aude Simon

Received: date / Accepted: date

Abstract This work is dedicated to the theoretical investigation of the influence of water clusters' organisation and size on the electronic spectrum of an interacting benzene (Bz) molecule using both TD-DFT and CASPT2 approaches. The geometries were extracted from two benzene-hexagonal ice configurations leading to maximum/minimum ionization energies (Geo_{IEI}/Geo_{IED} series) [1]. An appropriate basis set containing atomic diffuse and polarisation orbitals and describing the Rydberg states of Bz was determined. The TD-DFT approach was carefully benchmarked against CASPT2 results for the smallest systems. Despite some discrepancies, the trends were found to be similar at both levels of theory: the positions and intensities of the main $\pi \rightarrow \pi^*$ transitions were found slightly split due to symmetry breaking. For the smallest systems, our results clearly show the dependence of the electronic transitions on the clusters' structures. Of particular interest, a $\pi \rightarrow$ Rydberg orbital transition of non negligible oscillator strength, the Rydberg orbital being expanded on the water cluster, was found for the Geo_{IED} series only. It was found lower than 7 eV *ie* more than 2 eV below the ionization potential of Bz. When the cluster' size increases, similar transitions are found for all structures, the Rydberg orbitals becoming mainly developed on the H atoms of the water molecules at the edge of the cluster. Given their nature and energy, such

Nadia Ben Amor

Lab. Chim. & Phys. Quant. LCPQ IRSAMC, Univ. Toulouse UT3 & CNRS, UMR5626, 118
Route Narbonne, F-31062 Toulouse, France

Eric Michoulier

Lab. Chim. & Phys. Quant. LCPQ IRSAMC, Univ. Toulouse UT3 & CNRS, UMR5626, 118
Route Narbonne, F-31062 Toulouse, France

Aude Simon

Lab. Chim. & Phys. Quant. LCPQ IRSAMC, Univ. Toulouse UT3 & CNRS, UMR5626, 118
Route Narbonne, F-31062 Toulouse, France
E-mail: aude.simon@irsamc.ups-tlse.fr

transitions could play a role in the photochemistry of aromatic species in interaction with water clusters or ice, such processes being of astrophysical interest.

Keywords Excited states · Charge transfer state · Rydberg states · MS-CASPT2 · TD-DFT · Solvation · Benzene

1 Introduction

The study proposed in this paper is part of an ongoing effort aiming at understanding the physical and chemical processes following the photoactivation of carbon matter in interstellar space. In space, carbon is the fourth most abundant element and it is mainly present under the form of large carbonaceous molecules. [2] Among them, those possessing an aromatic character, Polycyclic Aromatic Hydrocarbons (PAHs), have received considerable interest since they were proposed, in the mid-eighties, as the carriers of the Aromatic Infrared Bands (AIBs), a set of mid-IR emission bands observed in many regions of the interstellar medium [3, 4]. This 'Astro-PAH' population would constitute about 10 to 20 percent of the total elemental carbon in the interstellar medium (ISM) [5, 6] although no specific PAH molecule has been identified yet [7]. Astro-PAHs may also play an important role in the chemistry of the ISM, sustaining interest for the investigation of their energetic processing (see reference [8] and references therein).

In dense interstellar clouds, where temperatures are low (< 50 K), molecular PAHs may condense onto the icy mantles of dust grains [9]. UV irradiation or energetic particle bombardment of these dust particles are expected to induce energetic processes leading to a specific chemistry within the ice [10]. This astrophysical context motivated experimental studies investigating the photoprocessing of PAHs in water ices upon UV irradiation under different conditions. Under high energy VUV irradiation, the formation of PAH cations was observed [11–13], as well as a rich photochemistry, leading to the formation of alcohols, quinones and ethers [14, 11, 15]. At lower energy ($\lambda > 235$ nm), the photoreactivity of pyrene and coronene with water molecules was observed in argon matrix or in Amorphous Solid Water (ASW) at 10 K [16–18] also revealing the production of oxygen-containing PAH products. Interestingly, this reactivity occurs at energies below the ionisation energy (IE) of isolated PAHs (~ 7.4 and 7.2 eV for pyrene and coronene, respectively). One hypothesis is that photoreactivity, even at lower energy, could be ion-mediated [13]. Experimental studies, complemented with modelling, showed that the ionisation of PAHs adsorbed on water ice required about 1.5 to 2.0 eV less energy than in the case of isolated PAHs [19, 20]. We showed using explicit description of the electrons within the Self Consistent Charge Density Functional based Tight Binding (SCC-DFTB) scheme [21–23], that this could not be accounted for by the only lowering of the ionisation energy, which was found less than 1 eV

[1]. A way to rationalize the experimental results would be to take into account the fact that the electrons released by the ionisation could attach to H_2O molecules or recombine with free radicals such as OH formed during ice photolysis [24] and to subtract the electron affinity of the electron receptor. An alternative hypothesis is the formation of a charge transfer (CT) $\text{PAH}^+-(\text{H}_2\text{O})_n^-$ electronic excited state [25] of sufficiently long lifetime to be detected and react.

In order to get insights into the possibility of formation of such state, we investigate the electronic excited states of a benzene molecule solvated by a series of $(\text{H}_2\text{O})_n$ clusters ($n < 50$), benzene being the simplest aromatic carbon molecule (quoted C_6H_6 or Bz hereafter). The vertical electronic spectra are computed at the Time Dependent Density Dunctional Theory (TD-DFT) and Multi-State Complete Active Space with Perturbation Theory at the second order (MS-CASPT2)[26] levels for the smallest clusters. The comparison between both approaches is mandatory, the presence of Rydberg and charge-transfer states in these systems requiring the use of adequate functionals and basis sets.

A few theoretical studies were dedicated to study the effect of the interaction of water clusters on benzene on the electronic spectrum of benzene. Vertical TD-DFT spectra of $\text{Bz}(\text{H}_2\text{O})_6$ were computed with the two conformations of the water hexamer, cage and prism [27], showing a red shift of the $\pi \rightarrow \pi^*$ transition of benzene. From their study, they conclude that benzene interaction with $(\text{H}_2\text{O})_6$ cluster plays a significant role in giving new excitation features in UV spectra of $\text{Bz}(\text{H}_2\text{O})_6$ clusters, and that charge transfer (CT) states and locally excited diffuse states play an important role in such systems. Interestingly, they show that the obtained electronic spectrum is dependent on the functional, and that MO62X and CAM-B3LYP generally show good agreement. They used the 6-31++G(d,p) basis set that is not expected to describe properly the Rydberg states of benzene but the authors do not focus on the correct description of the latter states. Sharma et al.[28] pursued their study expanding the benzene environment. They computed TD-DFT spectra of Bz adsorbed on Ih water ice using the ONIOM(QM:MM) formalism with the QM part at the MO62X/6-31++G(d,p) level and the MM part using AMOEBA09. Their conclusions regarding the electronic spectra was quite similar to their previous work[27], also showing the presence of Bz-mediated transition in the spectrum of water ice. Besides, they highlighted the dependence of the IE values and electronic spectra on the interface structure *ie* the presence of dangling OH (free OH on the ice surface). A few years later, Michoulier et al. generalized this study showing the dependence of the PAH-ice interaction energy on the structure at the interface for a series of PAH and ice types using a molecular dynamics/force field approach [29]. The dependence of the IE of the PAH on the PAH-ice structure at the interface was also shown using the self consistent charge density functional based tight binding approach (SCC-DFTB) [1].

The influence of the environment constituted of water clusters on the electronic spectra of carbonaceous aromatic species was also studied for small PAHs using quantum chemical calculations. Sharma et al. published a similar study as $\text{Bz}(\text{H}_2\text{O})_6$ [27] replacing benzene by naphthalene [30]. The influence of a water ice environment (modelled by about 40 water molecules) on the vibronic profile of the absorption spectrum and on the fluorescence spectrum of pyrene below 4.5 eV was studied through *ab initio* simulations [31].

In the present study, we report TD-DFT and MS-CASPT2 results for two series of $\text{Bz}(\text{H}_2\text{O})_n$ clusters ($n < 50$), differing by the organisation of the water molecules which, for one series, lead to an increase of the IE, and for the other one to a decrease of the IE. The geometries of the clusters, obtained at the SCC-DFTB level, were extracted from those determined in previous work [1] (see subsection 2.1). We showed in that study that an increase of the IE was due to the presence of interacting dangling OH while a decrease of the IE was due to the presence of interacting water oxygens. In the present work, we aim at determining the influence of the structural variations on the electronic spectrum, searching for a correlation between a decrease in the IE and the presence of low lying excited states with charge transfer from benzene to water clusters.

This article is organized as follows : the computational details including the benchmark on isolated benzene are reported in Section 2. The results for the two series of benzene-water clusters increasing the size of the water clusters are reported and discussed in Sections 3 and 4. Finally some conclusions are drawn in section 5.

2 Computational details

2.1 Systems

Before studying clusters involving several water molecules, we decided to calibrate methods and basis on benzene for which detailed experimental results exist and to investigate the effect of the coordination of one water molecule on the electronic spectrum of benzene considering two orientations (see Fig. 1) : Geo_{IEI-1} in which one of the hydrogen atoms of the water molecule interacts with the π cloud of benzene, leading to an increase of the VIE of +0.32 eV at the C-DFTB level of theory, and Geo_{IED-1} in which the oxygen atom interacts with the hydrogen atoms of benzene, leading to a decrease of the VIE of 0.33 eV at the C-DFTB level of theory. Experimental geometry was used for the benzene[32] while geometries of the two systems with one water molecule were optimized using the same C-DFTB potential as for the other clusters studied in this work for the sake of consistency.

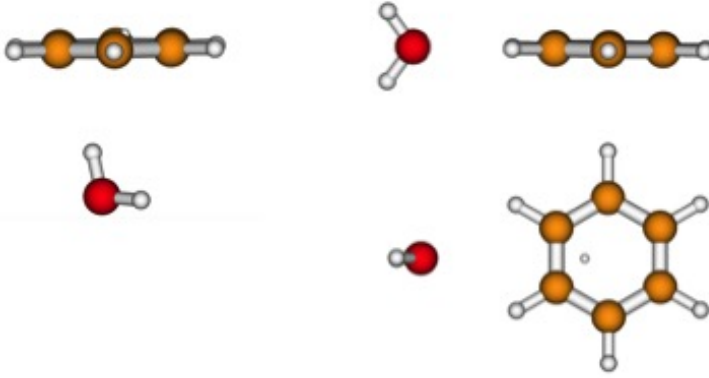


Fig. 1 Geometries locally optimized at the SCC-DFTB levels, namely Geo_{IEI-1} (left) and Geo_{IED-1} (right, side and top views)

The structures of the $(C_6H_6)(H_2O)_n$ ($n > 1$) clusters were extracted from larger systems containing more than 100 water molecules organized as hexagonal ice, optimized at the SCC-DFTB level of theory. [33,1]. We chose to study two series of systems: one for which the adsorption on ice leads to the maximum increase of the ionisation energy (" Geo_{IEI-n} " series) and, on the opposite, one for which the adsorption on ice leads to the maximum decrease of the ionisation energy (" Geo_{IED-n} " series) among all the series of "Bz-Ih" ice systems studied, all configurations differing by the local organisation at the Bz-ice interface [1].

In order to achieve electronic excited states calculations maintaining explicit electronic structure for all atoms, we had to reduce the size of the system. The truncations were achieved following the procedure detailed hereafter. Shells of decreasing radius were determined as follows: for a given water molecule, we defined the metric $d(CO)$ as the minimum distance between its oxygen atom and any of the carbon atoms of the benzene molecule. A water molecule was kept if $d(CO)$ was smaller than 8.0 (Geo_{IEI-49} and Geo_{IED-48}), 5.0 (Geo_{IEI-12} and Geo_{IED-14}) and 3.5 (Geo_{IEI-6} and Geo_{IED-5}) Å. The Geo_{IEI-n} Geo_{IED-n} geometries studied in this work are reported in Fig. 2. The vertical ionisation energies (VIEs) of the solvated benzene molecule was estimated using the constrained DFTB (C-DFTB) approach, previously used for the entire large system in ref [1]. We used the same parameterisation as in our previous work[1]. We must note that, with such parameterisation, the VIE of benzene is overestimated by 0.16 eV with respect to the experimental value, although in the case of pyrene, it was found equal [1].

All the geometries' cartesian coordinates are given in the Supplementary Information (SI).

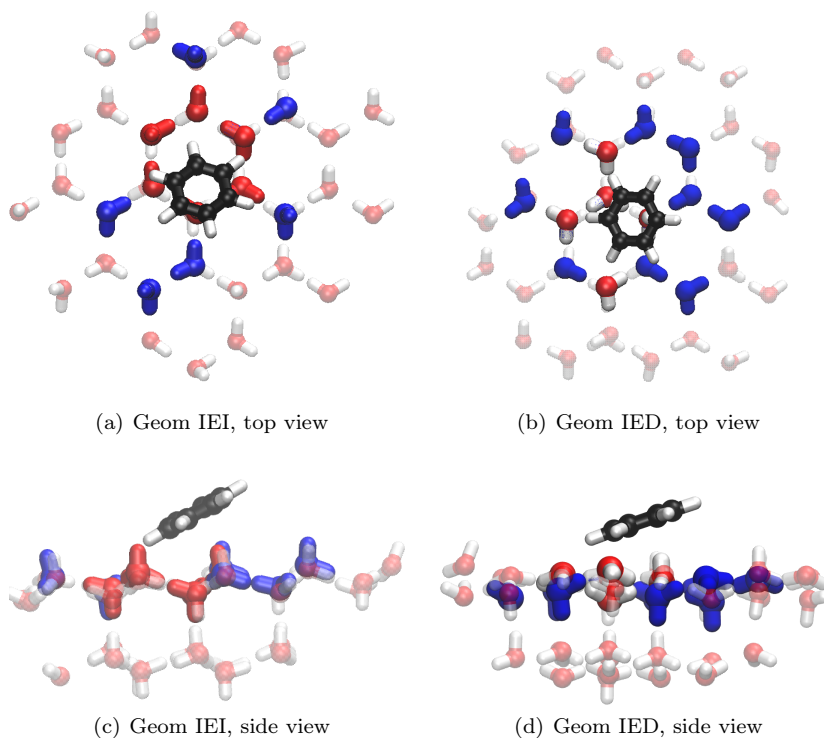


Fig. 2 Configurations were the vertical ionisation energy increases (IEI) and decreases (IED). Red water molecules correspond to the smallest configuration. Blue water molecules are the additional water molecules. And the transparent water molecules are the largest system treated with TD-DFT. Size of system for IEI : 6 ,12, 49 water molecules. Size of system IED : 5, 14, 48 water molecules

2.2 Electronic structure methods and basis sets

Complete Active Space Self Consistent Field [34] (CASSCF) and Multi-State Complete Active Space with Perturbation at the Second Order [26] (MS-CASPT2) methods have been used for the determination of the excitation energies of the smallest systems in order to get reference calculations to check the validity of the TD-DFT calculations when Rydberg or charge transfer states are present. The CASSCF/MS-CASPT2 calculations were carried out with the 7.8 MOLCAS package.[35–37] Atomic Natural Orbitals (ANO-L)[38] basis sets were used with the following contraction scheme: for C, N, O a (14s9p4d3f) set contracted to [3s2p1d] and for H a (8s4p3d) set contracted to [2s1p]. As Rydberg states are interleaved with valence states in benzene molecule, specific diffuse functions with small Gaussian exponents, in the average position of the two centers of charge of the cations coming from the two highest π orbitals of the benzene, were defined for each studied system[39]. The additional diffuse functions were obtained using exponents from the Kaufmann

series [40] and coefficients obtained from the genano module in MOLCAS[41]. All the coefficients were kept, as a very large number of Rydberg states are expected, not only those of the benzene molecule but also those of the increasingly numerous water molecules. Furthermore, all the states of isolated benzene are better described (see SI, table S1), even the valence states, while the Rydberg states are considerably affected. These coefficients were determined for each system and can be found in the SI. These basis sets are called Gen. in the tables.

The active space was defined to provide a good description of valence singlet states ($\pi \rightarrow \pi^*$) as well as the Rydberg states ($\pi \rightarrow Ry$). The same active space was defined for all systems, with all π orbitals of the benzene and one s, three p and five d Rydberg orbitals. However, include oxygen lone pairs in the active space is not feasible and the $n_O \rightarrow R_y$ states can not be described. State-average orbitals on 42 singlet states were optimized in order to obtain all the targeted states.

At the MS-CASPT2 level, the 34 lowest states were considered. The use of a level shift in the MS-CASPT2 method avoids weak intruder states by the addition of a shift parameter to the zeroth-order Hamiltonian. The value of this level shift has been chosen to obtain a stability of the excitation energies and a maximal deviation of 3% of the reference weight of the zeroth-order wave functions of the excited states compared to the ground state one, ie, 0.3 for the benzene and 0.4 for all other systems. Standard Ionization Potential-Electron Affinity (IPEA) shift in the perturbation treatment is used. The oscillator strengths were calculated thanks to the restricted active space state interaction approach (RASSI).[42]

The electronic spectra were also computed using the Time Dependent DFT methodology using the CAM-B3LYP functional [43], a long range corrected functional that was shown to provide satisfactory results for the description of low lying Rydberg states of PAHs [44] as well as Rydberg and charge transfer intra- and intermolecular states for a series of test molecules [45]. Two different basis sets were tested in the benchmark on the isolated benzene, the first one is the same than for the MS-CASPT2 calculation, named Gen., and the second one is a SVP+Diffuse basis[46] with diffuse functions placed at the average position of the centers of charge of the two cations coming from the benzene. These functions are those of the DZ+Double Rydberg defined for the carbon atom (2s2p2d)[46] with one additional f function (coefficient of 0.012). For all the other systems (benzene with water molecules), the basis set to describe the Rydberg orbitals is constructed by averaging the coefficients of the carbon and oxygen atoms. This second basis set is called DunRy (2s2p2d1f) in all the manuscript.

In order to characterize the CT character of the electronic excited states and in particular to investigate the "ghost state" character of the states we used descriptors namely the D_{CT} index [47] as implemented in Gaussian16 and the related M_{AC} (Mulliken average configuration) index [48]. The D_{CT} index quantifies the spatial extent associated to an electronic transition, hence it should provide indication on the CT character of the transition. For a given

transition, the comparison between the M_{AC} value and the energy should allow us to get insights into the potential "ghost state" character of the excited states. However, they have never been used to characterize the types of systems studied in the present paper, but more on extended delocalised systems. The D_{CT} and M_{AC} values were computed for all systems for the unrelaxed densities. When ghost states were suspected, these were reevaluated with the excited states relaxed densities to insure quantitative results [49].

The TD-DFT calculations and their related properties, natural transitions orbitals (NTOs) [50] and D_{CT} index, were computed using the Gaussian16 suite of programs[51]. The TD-DFT energies and excitations' detailed assignments, the shape of the MOs, a list of the transitions with the corresponding D_{CT} and M_{AC} index, as well as NTOs for Geo_{IEI-12} and Geo_{IEI-49} can be found in the .pdf files of the SI (see section 6).

All calculations have been carried out in the C_1 point-group symmetry.

2.3 Benchmark on benzene

To calibrate methods and basis sets, benchmark was achieved, using experimental results, on benzene (C_6H_6 , hereafter Bz). The geometry is taken from Hertzberg book[32] while the spectroscopic data arise from absorption spectra and multi-photon measurements [52–57].

The first calibration concerns the generation of ANO basis set for Rydberg states. As mentioned before, when only one contracted function is used for each angular momentum component, the error compared to the experimental values is considerably larger than when keeping all the functions (Table S1 in SI). In the case of the benzene, the generated basis set is composed of 3s3p4d orbitals. In a second time, the excited states have been determined with these basis sets but using TD-DFT with CAM-B3LYP functional. Except the first valence $\pi \rightarrow \pi^*$ excited state which is badly describe (error of 0.55 eV compared to experimental value), all the other states are found with a maximal error of 0.12 eV. One can note an admixture of valence and Rydberg states at 7.04 and 7.31 eV which does not occur in the MS-CASPT2 calculation. The corresponding oscillator strengths are then shared and lead to two absorption bands instead of one. The third test concerns the Rydberg basis sets when using TD-DFT method. As segmented and smaller basis set is preferable and even necessary to study the largest systems using Gaussian code, the DunRy (2s2p2d1f) basis set is compared to the previous one. The differences with experimental excitation energies are small, except for the first valence state, as previously, leading to a maximal deviation to the experimental values of 0.10 eV for all the other states. Same admixture of valence/Rydberg states is found again, in a lesser extent as the $\pi \rightarrow \pi^*$ is found at 6.99 eV instead of 7.04 with oscillator strength of 0.49 vs 0.44 for the Gen. basis set while the $\pi \rightarrow Ry(3p_z)$ is found at 7.27 eV instead of 7.31 with oscillator strengths of .14 instead of .18. At the MS-CASPT2 level, these two states were found at 6.91 eV (.80)

Transition Nature	MS-CASPT2/ Gen.	Gen.	TD-DFT/ DunRy (2s2p2d1f)	Exp. ^a
Valence states				
$\pi \rightarrow \pi^*$	4.97 6.20 6.91 (.80) 6.91 (.80)	5.45 6.17 7.04 (.44) 7.04 (.44)	5.46 6.16 6.99 (.49) VR 6.99 (.49) VR	4.90 6.20 6.94
$\pi (a_{2u}) \rightarrow \pi^*$	8.08			7.8
$\pi (a_{2u}) \rightarrow \pi^*$	8.10			
Rydberg states n=3				
$\pi \rightarrow 3s$	6.43 6.44	6.38 6.38	6.38 6.38	6.33
$\pi (a_{2u}) \rightarrow 3s$	9.28 (0.08)			
$\pi \rightarrow 3p(px, py)$	7.00 (.10) 7.07 (.002) 7.07 (.001) 7.14	6.89 (.07) 6.99 6.99 7.10	6.84 (.06) 6.94 6.94 7.05	6.93 6.95
$\pi \rightarrow 3p(pz)$	7.21 (.06) 7.22 (.05)	7.31 (.18) 7.31 (.18)	7.27 (.14) VR 7.27 (.14) VR	7.19
$\pi \rightarrow 3d(dz^2)$	7.57 7.57	7.48 7.48	7.47 7.47	7.54
$\pi \rightarrow 3d(dx^2 - y^2, dxy)$	7.66 7.67 7.73 7.73	7.57 7.57 7.58 7.58	7.52 7.53 7.55 7.55	7.46
$\pi \rightarrow 3d(dxz, dyz)$	7.89 7.91 7.91 7.94	7.78 7.78 7.78 7.83	7.70 7.71 7.71 7.75	7.81
VIE	9.26	9.25	9.26 (DFT) 9.40 (DFTB)	9.24

^a [52–57]

Table 1 MS-CASPT2/CAS(6,15) (DZP+Genano basis sets) / TD-DFT (CAM-B3LYP with Dunning-Hay Rydberg or Genano basis sets) results for C_6H_6 system. All excitations involved $\pi (1e_{1g})$ except if mentionned (in that case, excitations involved $\pi (a_{2u})$ orbital). VIE were determined using CAS(5,6)PT2 for two cations compared to the GS obtained with the CAS(6,6)PT2 calculation (CAS restricted to π orbitals)

and 7.21 eV (.06). All the methods and basis sets give very accurate vertical ionisation energy, with a maximal deviation of 0.02 eV.

Finally, the TD-DFT using CAM-B3LYP functional with SVP+diffuse Dunning-Hay basis sets for benzene and diffuse 2s2p2d1f functions to describe the Rydberg states gives on the benzene molecule very good results compared to experimental values, except for the first valence excited state. However, this state has no oscillator strength and is not decisive in the study of the effect of solvation on the electronic states. In view of these results, the following TD-DFT calculations will be performed within these basis sets.

3 Results

In this section, we present the electronic spectra of Geo_{IEI-n} and Geo_{IED-n} computed at the TD-DFT (CAM-B3LYP, $n < 50$) and MS-CASPT2 ($n \leq 6$) levels using the basis sets determined as explained hereabove. We chose to report in the main article the electronic spectra, the assignments of the transitions and some NTOs of interest. The details of the transitions that were found to be extremely multideterminantal, and the MOs are reported in the SI, along with the D_{CT} and M_{ac} indexes for all transitions of all systems. Only transitions with weights larger than 0.04 are taken into account to assign the nature of the transitions. The nature of the excited states is discussed in the lights of these analysis. All electronic spectra result from the convolution of the discrete spectra by a Lorentzian profile with a full width at half maximum of $1.7 \cdot 10^{-3}$ eV.

As we will compare some MS-CASPT2 and TD-DFT result, we must specify that, by construction, transitions from n_O orbitals are not described at the MS-CASPT2 level whereas they can be observed by essence at the TD-DFT level. Besides, regarding the MOs, and for all systems studied in the present work, a general observation is that more mixing between the different Rydberg orbitals, and also more valence-Rydberg mixing were found in TD-DFT calculations than in MS-CASPT2 calculations. However, local orbitals have been used in this latter case, which simplifies considerably the analysis by avoiding the mixing of the orbitals.

3.1 Geo_{IEI-1} and Geo_{IED-1}

The TD-DFT and MS-CASPT2 electronic spectra of Geo_{IEI-1} and Geo_{IED-1} along with that of Bz, are reported in Fig. 3. The assignments of the most intense bands are reminded. The analysis of the transitions (only the lowest energy ones of the TD-DFT spectra) are analysed in Table 2 for Geo_{IEI-1} and in Table 3 for Geo_{IED-1} , based on the transitions and molecular orbitals (MOs) reported in the SI (Geo_IEI-1.pdf and Geo_IED-1.pdf files). The NTOs corresponding to the lowest energy transitions describing electron transfer from π to Rydberg orbitals are reported in Figs. 4 and 5

At both levels of theory, we see that the effect of the adsorption of the water molecule on the electronic spectrum of benzene depends on their relative orientations.

In Geo_{IEI-1} , the position of the intense $\pi \rightarrow \pi^*$ transition is hardly affected by the interaction with the water molecule. A splitting due to symmetry breaking is observed. The difference between the TD-DFT and MS-CASPT2 level is that this splitting is slightly enhanced at the MS-CASPT2 level (6.98/6.99 eV vs 6.86/6.93 eV). The other intense transition at 7.15 eV at the TD-DFT level

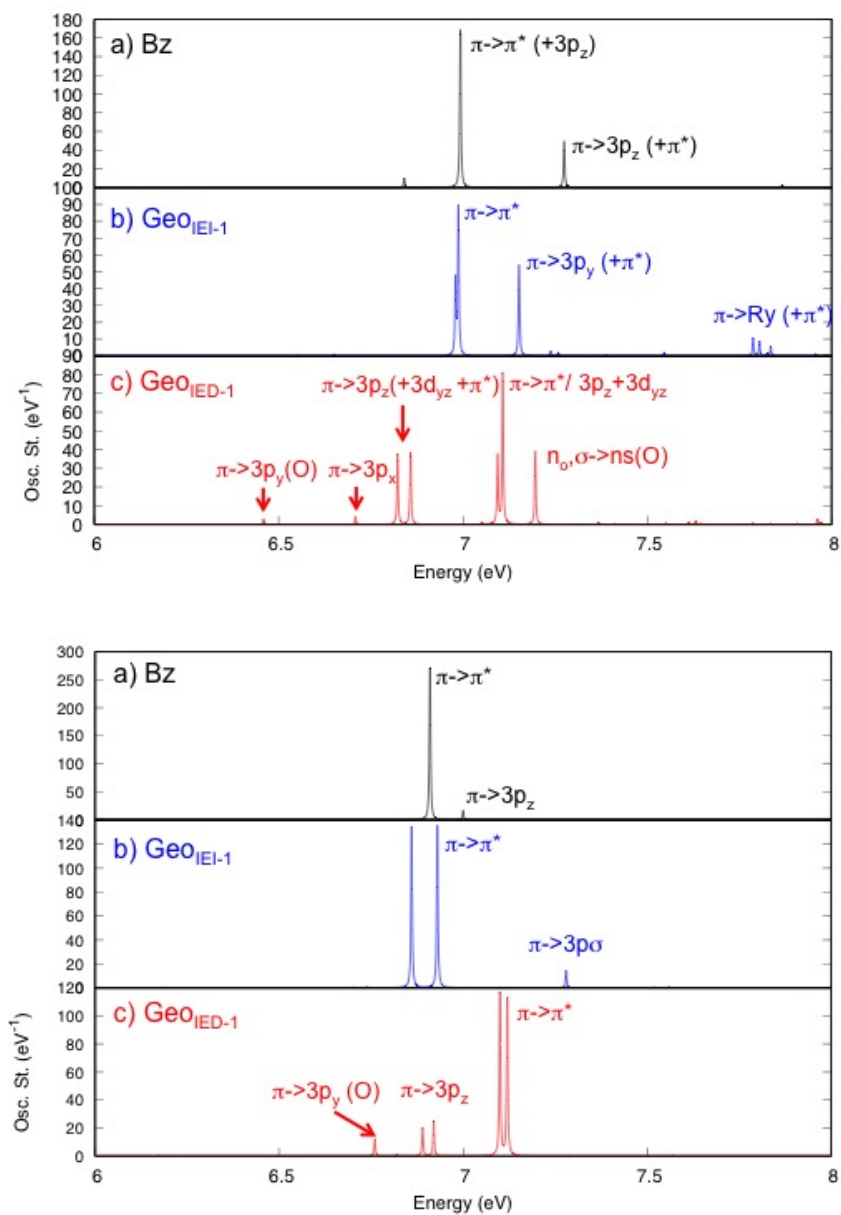


Fig. 3 Electronic spectra computed at the TD-DFT (top) and MS-CASPT2 (bottom) levels of theory and assignment of most intense transitions for a) B (black), b) and c) : $Bz - H_2O$ in Geo_{IEI-1} (b, blue) and Geo_{IED-1} (c, red)

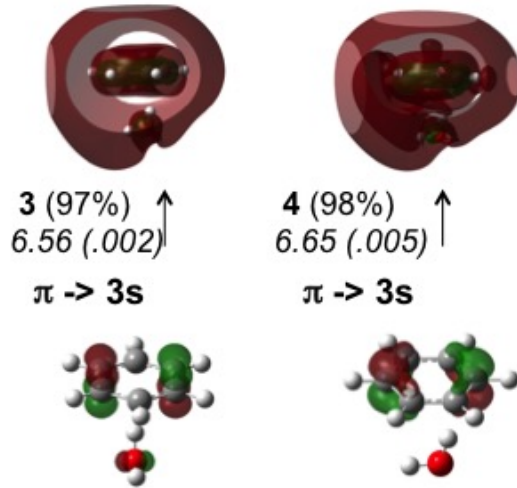


Fig. 4 NTOs (isovalues for MO surfaces of .08 for the HOMOs and .01 for the LUMOs) involved in the lowest energy in Geo_{IEI-1} (see (b) in Fig. 3 and assignment of transitions in table 2. Are also reported : the number of the transition, the contribution of the transition described by the NTOs with respect to the complete excited state (in %). The energy of the transition (in eV) and in oscillator strength are reminded in italics, the latter being in parenthesis. Only these two transitions could be reasonably represented by NTO transitions, the others are too multireferential maybe remove this figure.

is a transition from π electrons to mixed Rydberg $3p_y$ and valence π^* orbitals whereas the similar MS-CASPT2 state, although not mixed $\pi \rightarrow 3p_\sigma$, is observed at 7.28 eV. It is however satisfactory to see that all the states can be identified with deviations similar to those seen in benzene.

In Geo_{IED-1} , the intense $\pi \rightarrow \pi^*$ transitions are split and shifted towards higher energy at both MS-CASPT2 and TD-DFT levels. The blue-shift is larger at the MS-CASPT2 level (7.10/7.12 eV vs 6.91 eV in the case of Bz) than at the TD-DFT level (7.09/7.11 eV vs 6.99 eV compared to Bz). The splitting is the same for both methods. Interestingly, contrary to Geo_{IEI-1} , low energy transitions corresponding to a promotion of an electron from a π orbitals to a $3p$ (and $3s$ for TD-DFT) Rydberg orbitals located on the water molecule are found at both levels of theory, with non negligible intensities for a $\pi \rightarrow 3p_y(O)$ transition at the MS-CASPT2 level (6.76 eV) and one similar transition at 6.46 eV at the TD-DFT level (see NTO 5 on Fig. 5). Besides, an intense transition from the n_O orbitals of the water molecule (combined with σ_{CH}) to a Rydberg orbital centered on the O atom is seen at 7.20 eV. Removing the Bz molecule, such $n_O \rightarrow Ry(3s)$ was found at 7.03 eV (.06) for the water molecule in the same geometry as in Geo_{IED-1} . For Geo_{IEI-1} there is only a small contribution of the $n_O \rightarrow Ry$ excitation in the $\pi \rightarrow \pi^*$ state at 6.98 eV. The corresponding Rydberg state in the water molecule in the same geometry is found at 6.99 eV (.05).

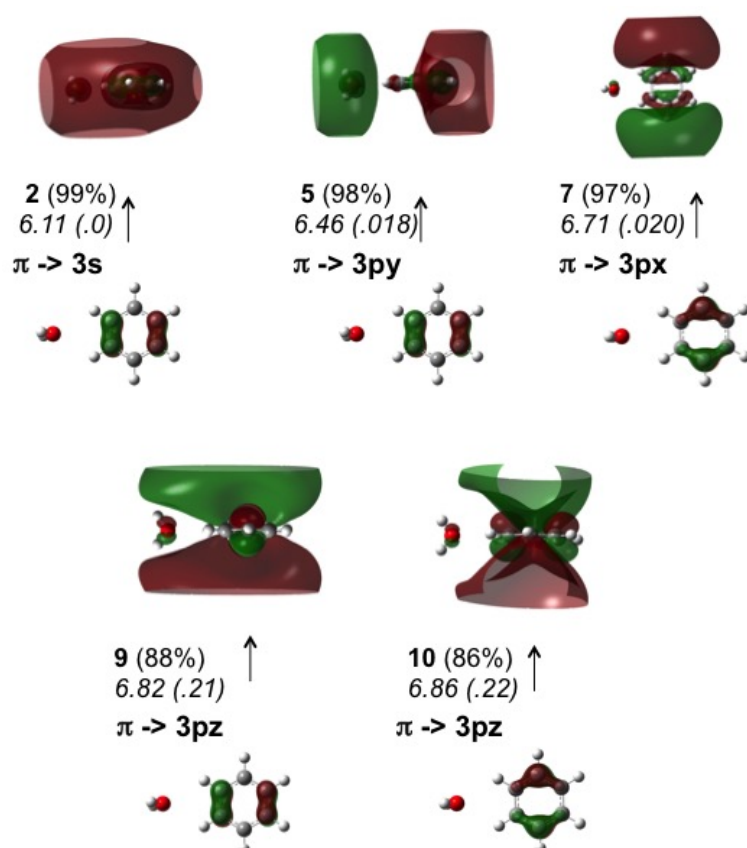


Fig. 5 NTOs (isovalues for MO surfaces of .08 for the HOMOs and .01 for the LUMOs) involved in the lowest energy and most intense transitions in Geo_{IED-1} (see (c) in Fig. 3 and assignment of transitions in table 3. Are also reported : the number of the transition, the contribution of the transition described by the NTOs with respect to the complete excited state (in %). The energy of the transition (in eV) and the oscillator strength are reminded in italics, the latter being in parenthesis.

This study on the Bz-H₂O isomers shows the influence of the position and orientation of the water molecule on the spectrum of Bz. Although differences are observed between the MS-CASPT2 and the TD-DFT results due in particular to more valence Rydberg mixing and the description of transitions from n_O orbitals in the latter case, the observed trends are similar. The valence $\pi \rightarrow \pi^*$ states are very similar to the isolated Bz in the case of Geo_{IEI-1} while the excitation energies of the third and fourth states are increased for the Geo_{IED-1} (7.10 instead of 6.94 eV). Rydberg states are found at higher energies (+0.3 eV) for Geo_{IEI-1} and lowered ones for Geo_{IED-1} (between -0.2 eV for 3s and -0.5 eV for 3d). Of particular interest, low energy charge transfer states resulting from the excitation of one electron in a π orbital of Bz to a Rydberg orbital located on the water molecule are observed for Geo_{IED-1} and

Transition Nature	<i>Geo_{IEI-1}</i>	
	MS-CASPT2/Gen.	TD-DFT/DunRy (2s2p2d1f)
Valence states		
$\pi \rightarrow \pi^*$	4.94 (0.001) 6.19 (0.002) 6.86 (0.790) 6.93 (0.793) 8.14	5.47 6.17 6.98 (.26) 6.99 (.48)
$\sigma \rightarrow \pi^*$		7.87
Rydberg states		
$\pi \rightarrow 3s$	6.70 (0.004) 6.74 (0.005) 9.53 (0.070)	6.56 (.002) 6.65 (.005)
$\pi \rightarrow 3p(px, py)$	7.28 (0.084) 7.31 7.33 7.43	7.24 (.017) 7.26 (.012) 7.39 (.002)
$\pi \rightarrow 3p(pz)$	7.52 (0.003) (3p _z /O) 7.56 (0.005)	7.51 (+3basis3dxz) 7.55 (.01 (+3basis3dxz))
$\pi \rightarrow 3d$	7.92 (.001) (3d _{z²}/O) 7.96 (3d_{xy}) 8.01 (.001) (3d_{xy}) 8.01 (3d_{x²-y²) 8.02 (3d_{x²-y²) 8.03 (.001) (3d_{z²}/O) 8.26 (3d_{xz,yz}) 8.28 (.001) (3d_{xz,yz}) 8.32 (.003) (3d_{xz,yz}) 8.32 (3d_{xz,yz})}}}}	7.75(+s,p,f) 7.80 (.01) 7.89 (+p,f) 7.90 (+s,p,f)
Rydberg/Valence states		
$\pi \rightarrow \pi^*/Ry$	8.00 (3d _{xy})	7.15 (.16) (3py + π^*) 7.15 (.16) (3py + π^*) 7.69 (4s + 4px + 3d) 7.79 (.06, d) 7.80 (.05, (p,(d,f))) 7.83 (.03, (d,p,s))
VIE	9.59	9.59 (DFT)/ 9.72 (C-DFTB)
VIE2	9.65	

Table 2 MS-CASPT2 and TD-DFT results for local minimum of C₆H₆/(H₂O) system in *Geo_{IEI-1}*. Vertical ionization energy (VIE) in second column computed at the SCC-DFTB level using charge constraint (method benchmarked in reference [1])

not for *Geo_{IEI-1}*.

3.2 Increasing the number of water molecules

In this subsection, we consider the clusters of Bz interacting with an increasing number of water molecules following the two series of geometries *Geo_{IEI-n}*

Transition Nature	<i>GeoIED-1</i>	
	MS-CASPT2/Gen.	TD-DFT/DunRy (2s2p2d1f)
Valence states (mixed with Ryd. in TD-DFT)		
$\pi \rightarrow \pi^*$	4.97 6.17 (.003) 7.10 (0.681) 7.12 (0.657)	5.45 6.14 7.09 (.21, + 3pz+ 3dyz) 7.11 (.46, + 3pz+ 3dyz)
Rydberg states		
$\pi \rightarrow 3s$	6.26 6.28	6.12 ($\rightarrow 3s$ (O) + 3py) 6.17 ($\rightarrow 3s$ (O) +3py)
$\pi \rightarrow 3p(px, py)$	6.76 (.069) (3py (O)) 6.81 6.82 (.005) 6.87 (3py (O))	6.46 (0.018, $\rightarrow 3py$ (O) + 3s (O) + 3dx2 - y2) <i>/6.56 ($\rightarrow 3s$ (O) +3py)/</i> 6.71 (.02, 3px + 3dxy) 6.77 (3px + 3dxy)
$\pi \rightarrow 3p(pz)$	6.89 (0.119) 6.92 (0.147)	6.82 (.21, + π^* + 3dyz) 6.86 (.22, + π^* + 3dyz)
$\pi \rightarrow 3d\sigma$	7.29 (.002) 7.34 7.41 7.45	7.05 (.006, 3dx2 - y2 +4s+4f) 7.11(3dx2 - y2 +4s) 7.23 (3dxy +3px + 4f) 7.25 (3dz2 +3px + 4f) 7.28 (3dz2 +3px + 4f) 7.29 (3dxy + 3dz2 +3px + 4f)
$\pi \rightarrow 3d\pi$	7.37 (dz2) 7.37 (dz2) 7.50 (basis3dyz) 7.55 (basis3dyz/basis3dxz) 7.57 (.002) (basis3dxz) 7.57 (basis3dxz/basis3dyz)	7.31 (3dyz+3pz + π^*) 7.37 (.007, 3dxz+3pz + π^*) 7.41 (.002,3dxz) 7.43 (3dxz)
$n_O, \sigma_{Bz} \rightarrow 3s(O) + 4s(O)$		7.20 (.22)
VIE	8.91	8.91 (DFT)/9.07 (C-DFTB)
VIE2	8.94	

Table 3 MS-CASPT2 and TD-DFT results for local minimum of $C_6H_6/(H_2O)$ system in *GeoIED-1*. VIE : vertical ionization energy. The analysis was achieved up to the 23rd state at the TD-DFT level. The transitions in brackets and in italics refer to "ghost states" as detected following the procedure indicated in Section 2.2.

and *GeoIED-n* as described in subsection2.1.

3.2.1 $Bz - (H_2O)_n$: *GeoIEI-6* and *GeoIED-5*

In this section, we present the electronic excited states of Bz interacting with 5 and 6 water molecules (*GeoIED-5* and *GeoIEI-6*) organized following the two configurations shown in Fig. 6.

The MS-CASPT2 and TD-DFT electronic spectra are reported in Fig. 7. The nature of the electronic transitions at both levels of theory, is detailed in Tables 4 and 5. Some NTOs of interest are reported in Figs. 8 and 9. The

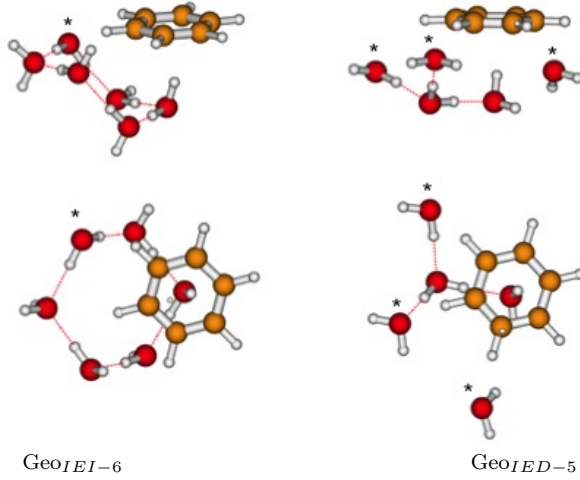


Fig. 6 Geometries with the smallest shell of water molecules, extracted from the two Bz-Ih ice structures, one leading to the maximum ionization energy (Geo_{IEI-n} series), the other one leading to the minimum ionization energy (Geo_{IED-n} series). The oxygen pointing towards benzene are designated with the \star symbol

details of the assignments of the transitions, the MOs, as well as the D_{CT} and M_{AC} indexes are reported in the SI ($Geo_IEI-6.pdf$ and $Geo_IED-5.pdf$ files).

Interestingly, both Geo_{IEI-6} and Geo_{IED-5} were found to have similar IEs, at the C-DFTB level of theory. The IEs of Geo_{IEI-6} were even found slightly smaller than those of Geo_{IED-5} at the MS-CASPT2 level of theory (see last line of Tables 4 and 5. This is the opposite of the largest structures that they have been extracted from, likely because a water molecule, as in Geo_{IEI-1} , interacts with Bz through its H atom pointing towards the π cloud of Bz for the two structures.

As can be seen in Fig. 7, the TD-DFT electronic spectra present more transitions with non negligible oscillator strengths than at the MS-CASPT2 level. Indeed, several transitions from n_O orbitals and from both π and n_O orbitals now come into play. For the two Bz-(H_2O) $_n$ clusters, the TD-DFT excitation energies of the water clusters without the benzene molecule were computed maintaining the presence of the Rydberg basis set, showing the presence of the expected bands (see Tables S2 and S3 of the SI). The excitation energies are more different for Geo_{IED-5} than for Geo_{IEI-6} . The nature of the excitations has been carefully checked for the latter one and (H_2O) $_6$ while in Geo_{IED-5} and (H_2O) $_5$ the mixing is too important to attribute with certainty the $n_O \rightarrow Ry$ transitions according to the contributions of the different oxygen atoms. However, from this comparison (SI, tables S2 and S3), in both cases, the $n_O \rightarrow Ry$ transitions of the water clusters clearly appeared in the Bz-clusters at

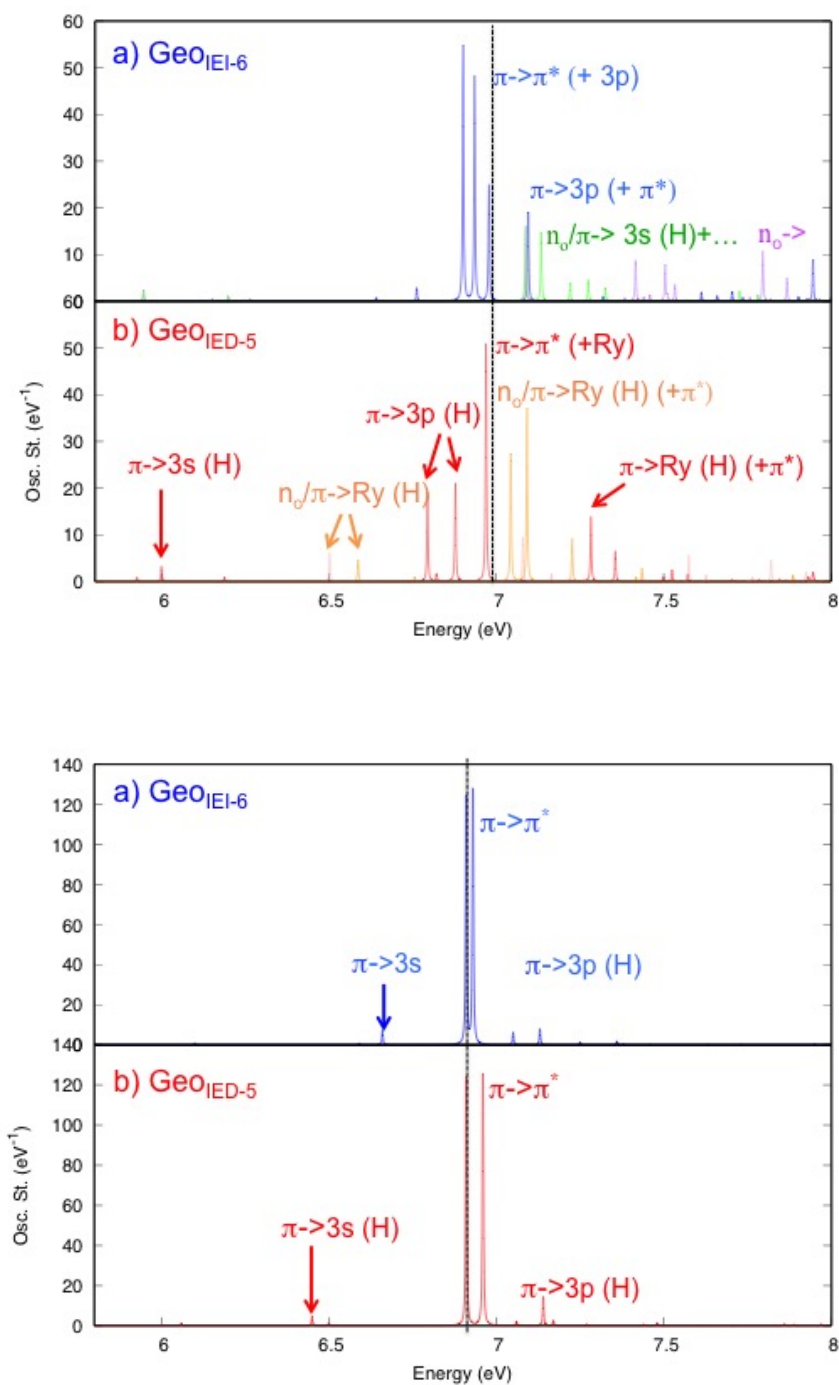


Fig. 7 TD-DFT electronic spectra (50 states, top) and MS-CASPT2 spectra (bottom) of Geo_{IEI-6} (a) and Geo_{IED-5} (b). For TD-DFT spectra, the use of different colors allow to distinguish between transitions from π , n_o and both (n_o , π) orbitals. The $\pi \rightarrow \pi^*$ transition energy for benzene is reported in dashed line.

close energies (0.1-0.2 eV).

Regarding the most intense $\pi \rightarrow \pi^*$ transitions, their position is hardly affected as they undergo splitting due to symmetry loss. At the MS-CASPT2 and TD-DFT levels, this splitting leads to the appearance of a band at slightly higher energy than that of Bz for Geo_{IED-5} whereas for Geo_{IEI-6} , at the TD-DFT level, it leads to new bands at slightly lower energy. Regarding the values of the splitting, they were found identical (0.05 eV) at the two levels of theory for Geo_{IED-5} : the two bands are located at 6.91 and 6.96 eV vs 6.91 eV for the isolated Bz at the MS-CASPT2 level, and at 6.97 and 7.04 eV vs 6.99 eV at the TD-DFT level. The results are slightly different for Geo_{IEI-6} as hardly any splitting was found at the MS-CASPT2 level (6.91 and 6.93 eV vs 6.91 eV for Bz) and three bands were found at 6.90, 6.93 and 6.98 eV ie -0.09, -0.06 and -0.01 eV with respect to the band of isolated Bz. In fact, only two bands correspond to the $\pi \rightarrow \pi^*$, but the three transitions are mixed. However, the last one, at 6.98 eV, presents a more pronounced $\pi \rightarrow Ry$ character than the two others.

Regarding Geo_{IED-5} , two $\pi \rightarrow 3s(H)$ transition at 6.45 eV and 6.50 eV were found at the MS-CASPT2 level of theory whereas those of similar nature were observed at the TD-DFT level at lower energies, 5.93 and 6.00 eV. In isolated Bz, these transitions were found at 6.33 eV. This difference is one of the largest between the two methods. In Geo_{IED-5} , several transitions involve both n_O and π valence orbitals, as well as both Rydberg and π^* virtual orbitals. There are also two more intense $\pi \rightarrow 3p(H)$ at 6.79 and 6.87 eV, that we checked do not correspond to the population of ghost states (see SI, last table in the `Geo_IED-5.pdf` file). Such transitions were observed at slightly higher energy at the MS-CASPT2 level (several bands around the most intense at 7.14 eV), which is above the $\pi \rightarrow \pi^*$ transition but remains much below the IP of Bz. In the case of Geo_{IEI-6} , $\pi \rightarrow Ry(3p)$ transitions were found slightly more intense than in the isolated benzene, at 6.98 eV (mixed with $\pi \rightarrow \pi^*$) and 7.10 eV.

The analysis of the TD-DFT transitions revealed quite complex. For these systems and all the more as the size of the water cluster increases, we found the lowest energy unoccupied MOs developed on the Rydberg basis set also have significant contributions on diffuse orbitals and especially the 3s orbitals of H atoms (belonging to some water molecules). This important contribution of the H atoms is quoted as /H in the tables and (H) in the figures. The 4p of the C and O orbitals, and to a lesser extent the 3s orbitals on the O atoms, also have non negligible contributions.

In regards with our goal of investigating charge transfer $Bz^+-(H_2O)_n$ states, the interesting result for such systems is the presence for Geo_{IED-5} , at both levels of theory, of $\pi \rightarrow Ry(H)$ transitions of non negligible oscillator strength, at lower energy than the intense $\pi \rightarrow \pi^*$ transition. As can be seen regarding

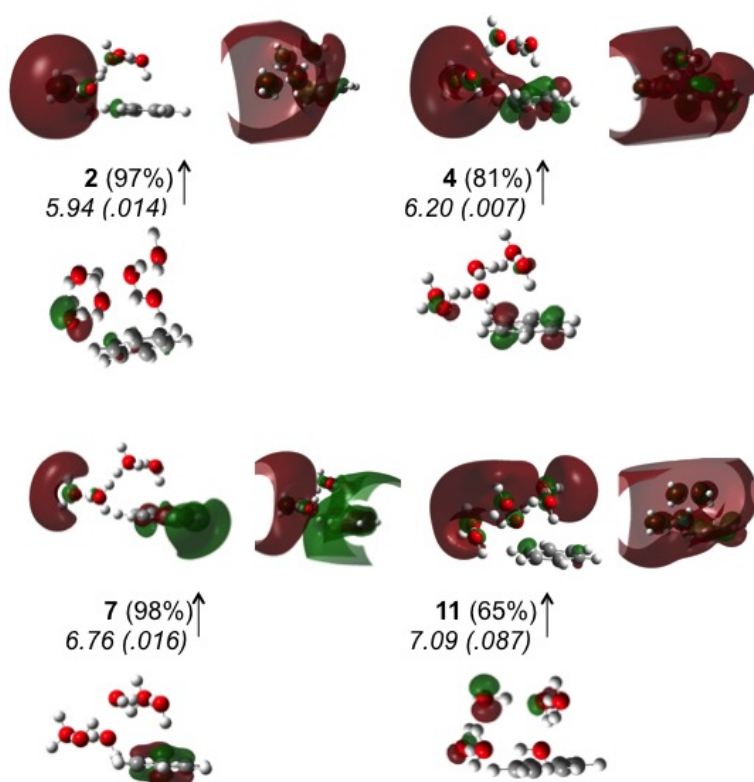


Fig. 8 NTOs for lowest energy transitions involving electron transfer to a Rydberg orbital located on the water cluster for Geo_{IEI-6} . HOMOs are drawn with a contour of .08 or .07, LUMOs with a contour of .02 and .005. Are also reported : the number of the transition, the contribution of the transition described by the NTOs with respect to the whole excited state (in %). The energy of the transition (in eV) and in oscillator strength are reminded in *italics*, the latter being in parenthesis.

the corresponding NTOs reported in Fig. 9, that of transition 8 is developed in particular on the water molecule whose oxygen point towards an H atom of the benzene molecule, which can be regarded as the counterpart of transition 5 for Geo_{IED-1} (see Fig. 5). The D_{CT} value for this transition is 3.22 Å, which falls into the maximum of the D_{CT} values' distributions which are reported for all systems in Fig. 10. Interestingly, in the case of Geo_{IEI-6} , an analogous transition is transition 7 at 6.76 eV (see Fig. 8) but its D_{CT} value is small (0.70 Å see SI, last table of $Geo_IEI-6.pdf$ file)).

Actually the D_{CT} values for Geo_{IEI-6} are globally smaller than the values of Geo_{IED-5} (see Fig. 10). Besides, contrary to Geo_{IED-5} , some ghosts states were identified among the lowest energy transitions), and this is the case for the transition 2 reported in Fig. 8. whereas that of transition 4 is not that clear (see SI, last table of $Geo_IEI-6.pdf$ file).

MS-CASPT2/Gen.		<i>Geo</i> _{IEI-6}	
Transition Nature	Exc. energy (eV)	TD-DFT/DunRy (2s2p2d1f)	Exc. energy (eV)
$\pi \rightarrow \pi^*$	4.98 (.001)	$\pi \rightarrow \pi^*$	5.47 (.001)
$\pi \rightarrow \pi^*$	6.10 (.006)	<i>n_O and $\pi \rightarrow Ry(3s)/H$</i>	<i>[5.94 (.014)]</i>
$\pi \rightarrow Ry(3s)$	6.59 (.004)	$\pi \rightarrow \pi^*$	6.15 (.003)
$\pi \rightarrow Ry(3s)$	6.66 (.042)	$\pi(+n_O) \rightarrow Ry(3s)/H + \pi \rightarrow \pi^*$	6.20 (.007)
$\pi \rightarrow \pi^*$	6.91 (.723)	$\pi \rightarrow Ry(3s)/H$	<i>[6.26 (.002)]</i>
$\pi \rightarrow \pi^*$	6.93 (.746)	$\pi \rightarrow Ry(3p)$	6.64 (.004)
$\pi \rightarrow Ry(3p_y)/H$	7.05 (.036)	$\pi \rightarrow Ry(3p) + Ry(3s)/H$	6.76 (.016)
$\pi \rightarrow Ry(3p_y)/H$	7.13 (.046)	$\pi \rightarrow \pi^* + Ry(3p)$	6.90 (.30)
$\pi \rightarrow Ry(3p_x)$	7.25 (.008)	$\pi \rightarrow \pi^* + Ry(3p)$	6.93 (.26)
$\pi \rightarrow Ry(3p)/H$	7.36 (.011)	$\pi \rightarrow \pi^* + Ry(3p)$	6.98 (.135)
$\pi \rightarrow Ry(3p)$	7.38 (.002)	$n_O(+\pi) \rightarrow Ry(3s)/H + Ry(3p)$	7.09 (.087)
$\pi \rightarrow Ry(3p_z)/H$	7.46 (.001)	$\pi \rightarrow Ry(3p) + \pi^*$	7.10 (.11)
$\pi \rightarrow Ry(3d_{xy})$	7.63 (.001)	$\pi \rightarrow Ry(3p) + n_O \rightarrow Ry(3s)/H$	7.13 (.081)
$\pi \rightarrow Ry(3d_{xy})$	7.73 (.001)	$\pi(+n_O) \rightarrow Ry(s,p,d) + \pi^*$	7.22 (.022)
$\pi \rightarrow Ry(3d_{xz,yz})$	7.81	$n_O(+\pi) \rightarrow Ry(3s)/H + Ry(3p)$	7.27 (.025)
$\pi \rightarrow Ry(3d_{xz,yz})$	7.91	$\pi \rightarrow Ry(3p)$	7.32 (.006)
$\pi \rightarrow Ry(3d_{xz,yz})$	7.95 (.002)	$n_O + \pi \rightarrow Ry(3s)/H + Ry(3p)$	7.33 (.017)
$\pi \rightarrow \pi^* / Ry(3d_{z^2})$	8.00 (.001)	$n_O \rightarrow Ry(3p) + \pi^*$	7.38 (.004)
$\pi \rightarrow Ry(3d_{xz,yz})$	8.05 (.001)	$n_O \rightarrow Ry(3s)/H$	7.42 (.05)
$\pi \rightarrow Ry(3d_{x^2-y^2})$	8.08 (.001)	$\pi \rightarrow Ry(3d) + \pi^*$	7.43
$\pi \rightarrow Ry(3d_{z^2})$	8.10 (.001)	$n_O \rightarrow \pi^*$	7.44 (.005)
$\pi \rightarrow \pi^*$	8.12 (.011)	$n_O \rightarrow \pi^*$	7.46 (.008)
$\pi \rightarrow Ry(3d_{x^2-y^2})$	8.17	$n_O \rightarrow Ry(3s)/H$	7.50 (.042)
$\pi \rightarrow \pi^*$	8.19 (.002)	$n_O \rightarrow Ry(3s)/H + \pi^*$	7.51 (.006)
$\pi \rightarrow Ry(3s)$	9.42 (.048)	$n_O \rightarrow Ry Ry(3s)/H + Ry(3p)$	7.53 (.020)
VIE	9.24	VIE C-DFTB	9.46
VIE2	9.34		

Table 4 Analysis of the MS-CASPT2 and TD-DFT lowest energy transitions (up to the 25th excited state) for *Geo*_{IEI-6}. The transitions in brackets and in italics refer to "ghost states" as detected following the procedure indicated in Section 2. LUMO orbital : Ry (3s)/H.

3.2.2 $Bz - (H_2O)_n$: *Geo*_{IEI-12} and *Geo*_{IED-14}

Increasing the size of the water clusters leads to *Geo*_{IEI-12} and *Geo*_{IED-14} (see Fig. 11). The TD-DFT electronic spectra are reported in Fig. 12, and the assignments of the lowest energy transitions for both clusters are reported in Table 6 based on the transitions' detailed assignments and MOs detailed in the SI (*Geo*_IEI-12.pdf and *Geo*_IED-14.pdf files). A few NTOs are reported in Fig. 13.

Increasing the number of water molecules as specified in subsection 2.1 has hardly an effect on the $\pi \rightarrow \pi^*$ transitions which are split but whose positions remain close to that of benzene (less than .05 eV deviation). They are slightly

MS-CASPT2/Gen.		<i>GeoIED-5</i> TD-DFT/DunRy (2s2p2d1f)	
Transition Nature	Exc. energy (eV)	Transition Nature	Exc. energy (eV)
$\pi \rightarrow \pi^*$	4.99	$\pi \rightarrow \pi^* [V+R]$	5.47
		$\pi \rightarrow Ry (3s) / H$	5.93 (.005)
		$\pi \rightarrow Ry (3s) / H$	6.00 (.018)
$\pi \rightarrow \pi^*$	6.06 (.008)	$\pi \rightarrow \pi^* [V+R]$	6.19 (.005)
		$n_O \rightarrow Ry (3s + 3p) / H$	6.50 (.033)
		$\pi \rightarrow Ry (3p) / H + n_O \rightarrow Ry (3s) / H$	6.59 (.026)
$\pi \rightarrow Ry (3s) / H$	6.45 (.027)	$\pi \rightarrow Ry (3p) / H + n_O \rightarrow Ry (3s) / H$	<i>[6.75 (.006)]</i>
$\pi \rightarrow Ry (3s) / H$	6.50 (.009)	$\pi \rightarrow Ry (3p) / H$	6.79 (.108)
		$\pi \rightarrow Ry (3p + 3d)$	6.82 (.009)
		$\pi \rightarrow Ry (3p) / H$	6.87 (.120)
$\pi \rightarrow \pi^*$	6.91 (.727)	$\pi \rightarrow \pi^* [V+R]$	6.97 (.284)
$\pi \rightarrow \pi^*$	6.96 (.736)	$\pi \rightarrow \pi^* [V+R] / n_O \rightarrow Ry / H$	7.04 (.156)
$\pi \rightarrow Ry (3p) / H$	7.06 (.012)	$n_O \rightarrow Ry / H$	7.08 (.052)
$\pi \rightarrow Ry (3p) / H$	7.14 (.084)	$\pi \rightarrow Ry [V+R] / n_O \rightarrow Ry / H$	7.09 (.207)
$\pi \rightarrow Ry (3p) / H$	7.17 (.015)	$n_O \rightarrow Ry / H$	7.15 (.009)
$\pi \rightarrow Ry (3p) / H$	7.27 (.004)	$n_O \rightarrow Ry / H + \pi \rightarrow Ry (3p) / H$	7.23 (.050)
$\pi \rightarrow Ry (3p)$	7.44 (.004)	$n_O \rightarrow Ry / H$	7.26 (.003)
$\pi \rightarrow Ry (3p)$	7.48 (.009)	$\pi \rightarrow Ry$	7.28 (.075)
$\pi \rightarrow Ry (3d)$	7.61 (.001)	$\pi \rightarrow Ry / H + \pi^* [V+R]$	7.35 (.036)
$\pi \rightarrow Ry (3d)$	7.70 (.001)	$n_O \rightarrow Ry / H (+ \pi^*)$	7.42 (.006)
$\pi \rightarrow Ry (3d)$	7.83 (.001)	$n_O \rightarrow Ry / H (+ \pi^*)$	7.44 (.016)
$\pi \rightarrow Ry (3d)$	7.86 (.005)	$\pi \rightarrow Ry / H + \pi^* [V+R]$	7.50 (.006)
$\pi \rightarrow Ry (3d)$	7.89 (.004)	$\pi \rightarrow Ry / H + \pi^* [V+R]$	7.53 (.014)
$\pi \rightarrow Ry (3d)$	7.97 (.005)	$n_O \rightarrow Ry / H + \pi^* [V+R]$	7.54
$\pi \rightarrow Ry (3d)$	8.00	$\pi \rightarrow Ry / H + \pi^* [V+R]$	7.57 (.008)
$\pi \rightarrow Ry (3d)$	8.04 (.001)		
$\pi \rightarrow Ry (3d)$	8.06		
$\pi \rightarrow Ry (3d)$	8.10		
$\pi \rightarrow \pi^*$	8.17 (.014)		
$\pi \rightarrow \pi^*$	8.19 (.001)		
$\pi \rightarrow Ry (3s) / H$	9.23 (.050)		
VIE (π)	9.32	VIE	9.45 (C-DFTB)
VIE2 (π)	9.38		

Table 5 Analysis of the MS-CASPT2 and TD-DFT lowest energy transitions (up to the 25th excited state) for $C_6H_6/(H_2O)_5$ in *GeoIED-5*. TD-DFT calculations : the "3s" and "3p" refer to the LUMO (3s), LUMO+1 (3p Rydberg character). They are indicated when their contribution is major. In this system Rydberg orbitals are located on the water clusters (see Supp Info). This is indicated by / H. When mixtures between Valence and Rydberg contributions appear significant, [V+R] is added. The transitions in brackets and in italics refer to "ghost states" as detected following the procedure indicated in Section 2.2.

blueshifted in the case of *GeoIED-14*, one of them resulting for both π and n_o orbitals transition to a π^* orbital, and slightly redshifted in the case of *GeoIEI-12*. These bands are surrounded by more low intensity bands than in *GeoIED-5* and *GeoIEI-6* due to the increased number of transitions from n_o and transitions involving depletion of both π and n_o orbitals. We may note that, for such large systems, an accurate analysis of the Rydberg type orbitals becomes difficult as there is increasing mixing between Rydberg and diffuse orbitals.

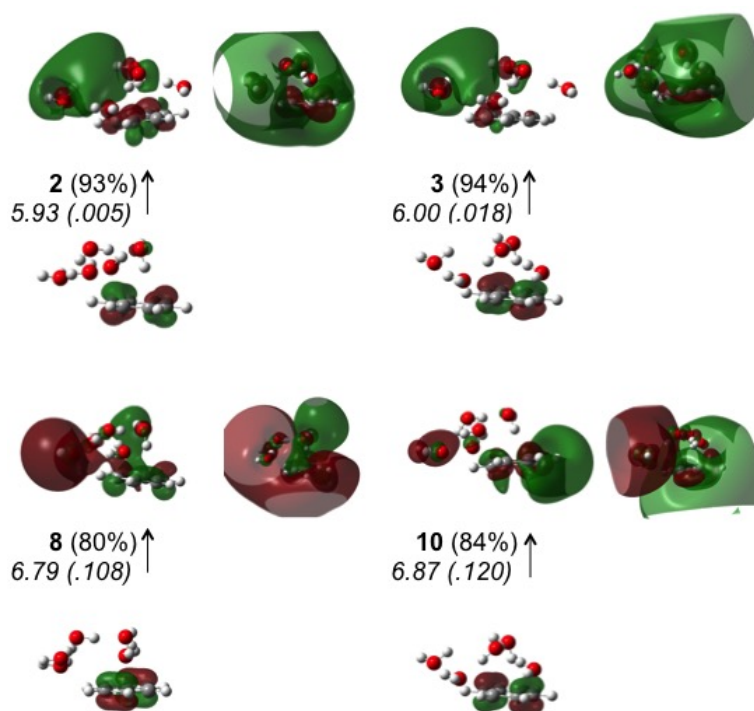


Fig. 9 NTOs for lowest energy transitions involving electron transfer from the π orbitals of benzene to a Rydberg orbital located on the water cluster for Geo_{IED-5} . HOMOs are drawn with a contour of .07 or .08, LUMOs with a contour of .02 and .005. Are also reported : the number of the transition, the contribution of the transition described by the NTOs with respect to the whole excited state (in %). The energy of the transition (in eV) and in oscillator strength are reminded in italics, the latter being in parenthesis.

For both Geo_{IED-14} and Geo_{IEI-12} , low energy transitions can be regarded as contributing to the population of $Bz^+-(H_2O)_n^-$ charge transfer states, although many of them are of negligible oscillator strength. However, for both structures, a few low lying excited states involving $\pi \rightarrow Ry/H$ transition of non negligible oscillator strength are involved, as for instance transition 14 for Geo_{IEI-12} and transition 17 for Geo_{IED-14} , whose NTOs are reported in Fig. 13, and whose energy remain below 7.0 eV, that is to say more than 2 eV below the IP of Bz. Interestingly, the MOs referred to as Rydberg MOs also have contribution on the diffuse H atoms of the water molecules located at the edge of the water cluster, leading to globally larger D_{CT} values. As for the other systems, the possibility of the presence of ghost states was investigated and the only suspected ghost state would be the 3rd one for Geo_{IED-14} (see the SI, Geo_IEI-14.pdf file). The D_{CT} value for this state is among the largest one for Geo_{IED-14} (5.37 Å), the D_{CT} values for transitions 6 and 17 were found to be ~ 3 Å, those for transitions 2, 5 and 14 of Geo_{IEI-12} were found to be 2.45, 3.41 and 1.13 Å respectively (for unrelaxed densities). Over-

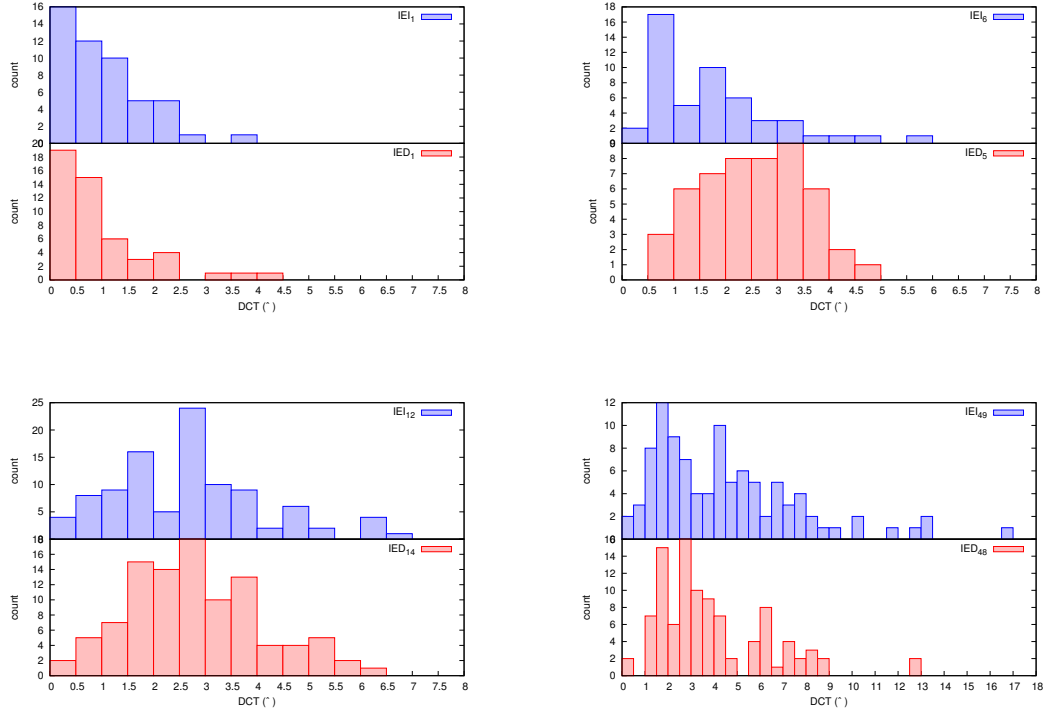


Fig. 10 D_{CT} indexes' distributions for all clusters with more than one water molecule studied in this work (see the SI for the assignment of the D_{CT} index to the corresponding transition).

all, as can be seen in Fig. 10, the D_{CT} values for Geo_{IED-14} and Geo_{IEI-12} are more spreaded towards larger distances than Geo_{IED-5} and Geo_{IEI-6} , illustrating the longer "distances" browsed by the electron upon excitation.

This study of intermediate-size systems confirms the dependence of the electronic spectrum on the organisation of the water molecules interacting with Bz. Interestingly, in the view of identifying low energy $Bz^+-(H_2O)_n^-$ CT states, our calculations show that a few real $\pi \rightarrow Ry(H)$ states with non negligible oscillator strengths are found for Geo_{IED-14} and Geo_{IED-12} . Increasing the size of the systems, an increasing number of occupied MOs are developed on both π and n_O orbitals and an increasing $n_O \rightarrow Ry$ transitions are found. The trends found for these intermediate geometries are going to be confirmed for the largest size studied in subsection 3.2.3

TD-DFT/DunRy (2s2p2d1f) 38-14H ₂ O		TD-DFT/DunRy (2s2p2d1f) 34-12H ₂ O	
Transition Nature	Exc. energy (eV)	Transition Nature	Exc. energy (eV)
$\pi \rightarrow \pi^*$	5.49	$\pi \rightarrow \pi^*$	5.48
$\pi \rightarrow Ry3s$	5.70		
$n_O / \pi \rightarrow Ry$	5.76		
$n_O / \pi \rightarrow Ry$	5.86 (.01)	n_O (HOMO) $\rightarrow Ry$	6.05 (.01)
$\pi \rightarrow \pi^*$	6.17	$\pi \rightarrow \pi^*$	6.17
$n_O \rightarrow Ry$	6.23 (.01)	$n_O \rightarrow Ry$	6.29 (.02)
$n_O \rightarrow Ry$	6.42	$\pi \rightarrow Ry$	6.31
$\pi \rightarrow Ry$	6.43	$\pi \rightarrow Ry$	6.42
$n_O \rightarrow Ry$	6.52 (.02)	$n_O / \pi \rightarrow Ry$	6.62 (.01)
$n_O / \pi \rightarrow Ry$	6.57	n_O (HOMO) $\rightarrow Ry$	6.69
$n_O / \pi \rightarrow Ry$	[6.59]	$n_O / \pi \rightarrow Ry$	6.70 (.02)
$n_O / \pi \rightarrow Ry$	6.61		
$n_O / \pi \rightarrow Ry$	6.68 (.02)		
$n_O / \pi \rightarrow Ry$	6.70 (.03)		
$n_O / \pi \rightarrow Ry$	6.73 (.01)		
$n_O / \pi \rightarrow Ry$	6.75 (.02)		
$\pi / n_O \rightarrow Ry$	6.76 (.02)	$\pi \rightarrow Ry$	6.74
$n_O / \pi \rightarrow Ry$	6.78	$n_O \rightarrow Ry$	6.78 (.05)
$n_O \rightarrow Ry$	6.83 (.03)	$n_O \rightarrow Ry$	6.82 (.01)
$n_O \rightarrow Ry$	6.85 (.02)	n_O (HOMO) $\rightarrow Ry$	6.86
$\pi \rightarrow Ry$	6.87	$\pi \rightarrow Ry$	6.91 (.13)
$n_O \rightarrow Ry$	6.95 (.04)		
$n_O \rightarrow Ry$	6.97 (.03)		
$n_O / \pi \rightarrow Ry$	6.98 (.06)		
$n_O / \pi \rightarrow Ry$	6.99 (.01)		
$\pi / n_O \rightarrow \pi^*$	7.00 (.32)	$\pi \rightarrow \pi^*$	6.96 (.30)
$\pi \rightarrow \pi^*$	7.04 (.33)	$\pi \rightarrow \pi^*$	6.97 (.27)
		n_O (HOMO) $\rightarrow Ry$	7.04
$n_O / \pi \rightarrow Ry$	7.10 (.11)	$n_O / \pi \rightarrow Ry$	7.07 (.11)
$\pi \rightarrow Ry$	7.13 (.01)	$\pi \rightarrow Ry$	7.11 (.10)
$n_O \rightarrow Ry$	7.15 (.02)	$\pi \rightarrow Ry$	7.13 (.06)
$n_O \rightarrow Ry$	7.19 (.02)		
$n_O \rightarrow Ry$	7.19 (.02)		
$n_O \rightarrow Ry$	7.23 (.05)		
$\pi \rightarrow Ry$	7.24 (.04)	$\pi \rightarrow Ry$	7.18
$n_O \rightarrow Ry$	7.25	n_O (HOMO) $\rightarrow \pi^*$	7.27 (.01)
$n_O \rightarrow Ry / \pi^*$	7.27		
$n_O / \pi \rightarrow Ry$	7.32	$\pi \rightarrow Ry$	7.27 (.06)
$n_O \rightarrow Ry$	7.34	$n_O \rightarrow Ry$	7.29 (.03)
$n_O \rightarrow Ry$	7.34	n_O (HOMO) $\rightarrow Ry$	7.30 (.02)
$n_O \rightarrow Ry$	7.36	n_O (HOMO) $\rightarrow \pi^*$	7.33 (.01)
$n_O \rightarrow Ry$	[7.37 (.03)]	$\pi \rightarrow Ry$	7.33 (.02)
$n_O \rightarrow Ry$	7.38 (.04)	$n_O \rightarrow Ry$	7.38
$n_O \rightarrow Ry$	7.40	n_O (HOMO) $\rightarrow \pi^*$	7.41
$\pi / n_O \rightarrow Ry$	[7.41]	$n_O \rightarrow Ry$	7.42 (.02)
		$n_O / \pi \rightarrow Ry$	7.43
		$n_O / \pi \rightarrow Ry$	7.45 (.03)
		$n_O / \pi \rightarrow Ry$ and π^*	7.50(0.02)
		$n_O \rightarrow Ry$	7.51
		$\pi \rightarrow Ry$	7.55
		$n_O / \pi \rightarrow Ry$ and π^*	7.56(0.01)
		$\sigma_{CH} \rightarrow \pi^*$	7.58
		$n_O \rightarrow Ry$	7.58
		$n_O \rightarrow Ry$	7.59 (.01)
		$n_O \rightarrow \pi^*$	7.60
		$n_O \rightarrow Ry$	7.62
		$n_O \rightarrow Ry$	7.64 (.07)
		$\pi \rightarrow Ry$	7.68 (0.02)
VIE	8.93 (C-DFTB)	VIE	9.57 (C-DFTB)

Table 6 Analysis of the TD-DFT lowest energy transitions for Geo_{IED-14} (up to the 40th excited state) and Geo_{IEI-12} (up to the 43th excited state). The transitions in brackets and in italics refer to "ghost states" as detected following the procedure indicated in Section 2.2.

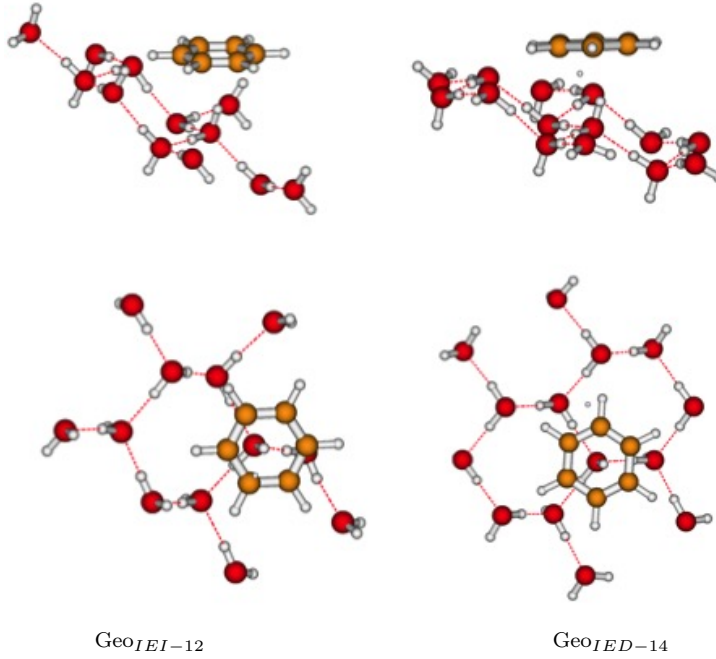


Fig. 11 Geometries extracted from the IEI (left) and IED (right) Bz-ice Ih structures containing respectively 12 and 14 water molecules.

3.2.3 Bz - (H₂O)_n : Geo_{IEI-49} and Geo_{IED-48}

The electronic spectra for Geo_{IEI-49} and Geo_{IED-48}, the largest systems studied in the present work, are reported in Fig. 14, the assignments of the lowest energy transitions are reported in Table 7. A few NTOs describing $\pi \rightarrow Ry/H$ transitions are reported in Figs. 15 and 16. All transitions' detailed assignments, MOs and D_{CT} and M_{AC} indexes are detailed in the SI (see files Geo_IEI-49.pdf and Geo_IED-48.pdf).

On the electronic spectra, we observe intense $\pi \rightarrow \pi^*$ dominant transitions slightly blueshifted - by less than .05 eV- with respect to that of benzene. Quasi no splitting (less than .02 eV) is found in the case of Geo_{IEI-48}, 0.04 eV for Geo_{IEI-49}. These intense excitations are not pure $\pi \rightarrow \pi^*$ as the latter are combined with $\pi \rightarrow Ry$ and $n_O \rightarrow Ry$ transitions. Interestingly, regarding these transitions, our results differ from those obtained by Sharma et al. [28] who computed a redshift of these bands with respect to those within isolated Bz when increasing the size of the water clusters, up to describing the Ih water ice environment using a QM/MM approach. However, as previously mentioned in the introduction, they used a different functional from ours (M062X, that is not a long range corrected functional) and a basis set that does not

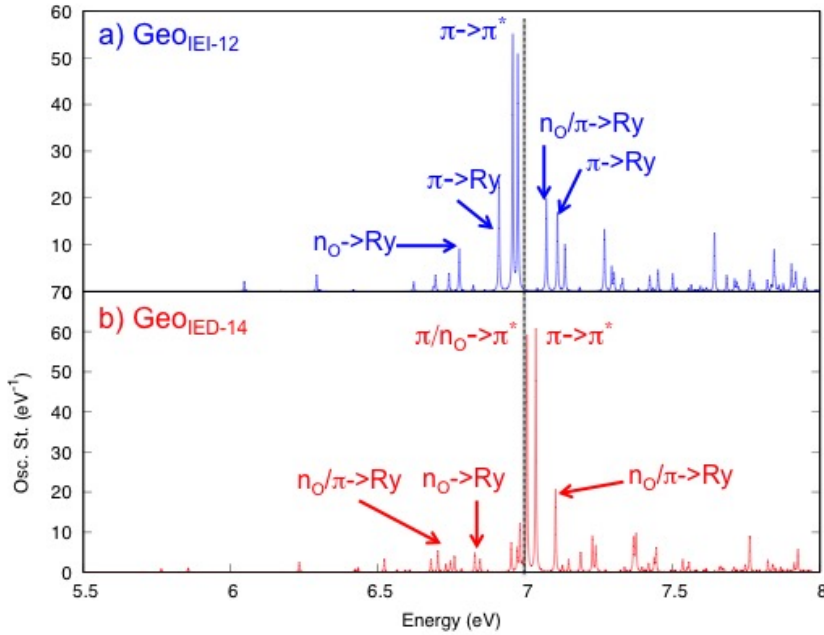


Fig. 12 TD-DFT electronic spectra (100 states) for *GeoIED-14* (red) and *GeoIEI-12* (blue).

describe the Rydberg states of Bz. These intense bands are surrounded by "seeds" ie numerous bands of weak intensities with oscillator strengths about ten times weaker. These transitions describe the promotion of one electron from n_O and π orbitals to Rydberg orbitals. Among those, some of them are suspected to be ghost states (see SI). In the case of $\pi \rightarrow Ry$ transitions of low energy for *GeoIED-48* at 5.84 to 6.05 eV) these suspected ghost states are of negligible oscillator strength.

As previously evoked in the case of smaller clusters, the MOs having a contribution on Rydberg AOs also have contribution on diffuse orbitals, in particular on the H atoms of water molecules located at the edge of the water cluster (see for instance the LUMOs of the transitions reported in Fig. 15). This is illustrated by the spreading of the D_{CT} index towards long distances (see Fig.10) up to 17 Å. A representative case is for instance the charge transfer $\pi \rightarrow Ry/H$ transition 3 of *GeoIED-48* which is characterized by a D_{CT} value of 7.1 Å. Transitions 36 and 40, more intense, are characterized by D_{CT} values of 2.6 and 3.8 Å. For the two geometries, low energy $\pi \rightarrow Ry$ transitions are present

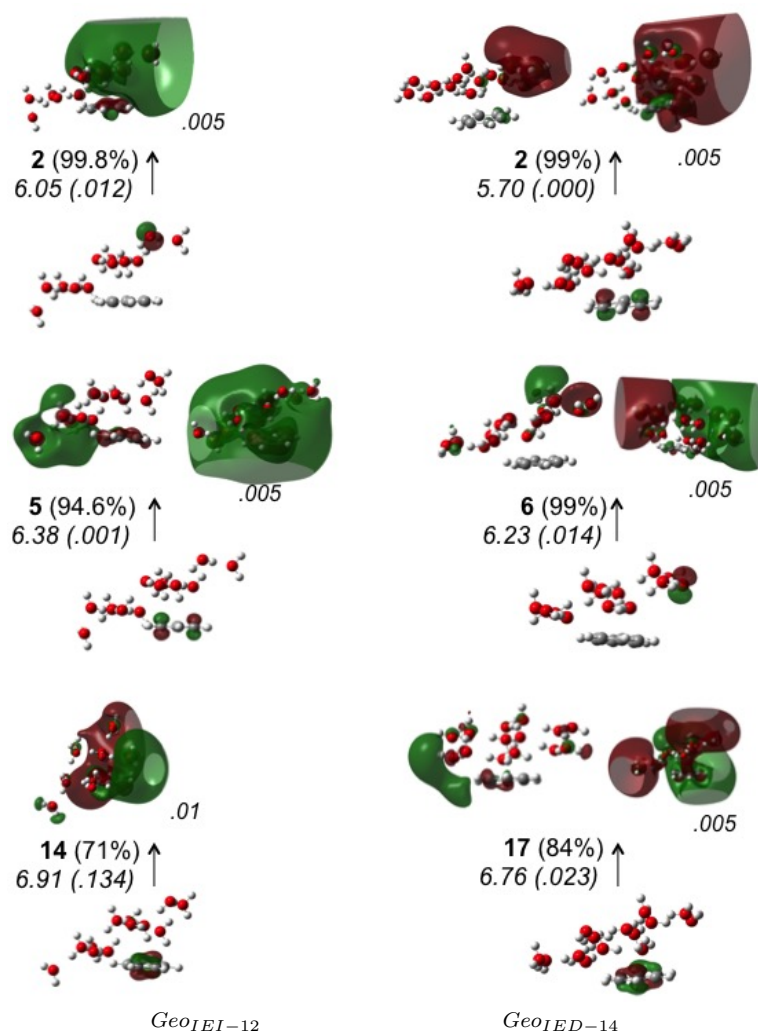


Fig. 13 NTOs related to a few low energy transitions for *GeoIEI-12* (left) and *GeoIED-14* (right). The HOMOs are drawn with a contour of .08, the LUMOs with a contour of .02 unless specified on the figure. Are also reported : the number of the transition, the contribution of the transition described by the NTOs with respect to the complete excited state (in %). The energy of the transition (in eV) and in oscillator strength are reminded in italics, the latter being in parenthesis.

and can be regarded as charge transfer $\text{Bz}^+ - [(\text{H}_2\text{O})_n]^-$ states. As mentioned previously, and contrary to the smallest cluster ($n=5,6$) the Rydberg states for such large systems are mostly located on the edge of the water clusters and are developed on both the Bz Rydberg orbitals and on the atomic diffuse orbitals located mostly on the H atoms of the water molecules at the edge of the cluster.

TD-DFT/DunRy (2s2p2d1f) Geo_{IED-48}		TD-DFT/DunRy (2s2p2d1f) Geo_{IEI-49}	
Transition Nature	Exc. energy (eV)	Transition Nature	Exc. energy (eV)
$\pi \rightarrow \pi^*$	5.50	$n_O (H) \rightarrow Ry$	5.28
$n_O (H-2) \rightarrow Ry$	5.77 (.01)	$\pi \rightarrow \pi^*$	5.49
$\pi \rightarrow Ry$	5.84	$n_O \rightarrow Ry$	5.99 (0.02)
$\pi \rightarrow Ry$	5.90	$n_O \rightarrow Ry$	6.02 (0.01)
$\pi \rightarrow Ry$	5.93	$\pi \rightarrow \pi^*$	6.18
$n_O (H-2) \rightarrow Ry$	5.96	$n_O (H) \rightarrow Ry$	6.33
$\pi \rightarrow Ry$	5.97	$n_O \rightarrow Ry$	6.33 (0.02)
$\pi \rightarrow Ry$	6.02	$n_O \rightarrow Ry$	6.41 (0.01)
$\pi \rightarrow Ry$	6.05	$n_O \rightarrow Ry$	6.42
$n_O \rightarrow Ry$	6.08 (.01)	$n_O (H) \rightarrow Ry$	6.45
$\pi \rightarrow \pi^*$	6.18	$\pi \rightarrow Ry$	6.47
$\pi \rightarrow Ry$	6.23	$n_O (H) \rightarrow Ry$	6.51
$\pi \rightarrow Ry$	6.28	$n_O \rightarrow Ry$	6.52 (0.02)
$\pi \rightarrow Ry$	6.32	$\pi \rightarrow Ry$	6.55
$\pi \rightarrow Ry$	6.36	$n_O (H) \rightarrow Ry$	6.62 (0.02)
$n_O \rightarrow Ry$	6.43 (.02)	$n_O \rightarrow Ry$	6.63 (0.01)
$\pi \rightarrow Ry$	6.47 (.01)	$n_O \rightarrow Ry$	6.64
$\pi \rightarrow Ry$	6.49 (.01)	$n_O (H) \rightarrow Ry$	6.67 (0.01)
$n_O \rightarrow Ry$	6.56 (.01)	$n_O \rightarrow Ry$	6.71 (0.03)
$n_O \rightarrow Ry$	6.58	$\pi \rightarrow Ry$	6.77 (0.08)
$\pi \rightarrow Ry$	6.62	$n_O \rightarrow Ry$	6.80 (0.01)
$n_O \rightarrow Ry$	6.66 (.01)	$n_O \rightarrow Ry$	6.81
$\pi \rightarrow Ry$	6.66	$n_O (H) \rightarrow Ry$	6.83
$n_O \rightarrow Ry$	6.68 (.01)	$n_O \rightarrow Ry$	6.84
$\pi \rightarrow Ry$	6.75 (.01)	$\pi \rightarrow Ry$	6.85 (0.04)
$\pi \rightarrow Ry$	6.81	$n_O \rightarrow Ry$	6.86 (0.01)
$n_O \rightarrow Ry$	6.82 (.02)	$n_O \rightarrow Ry$	6.87 (0.02)
$n_O \rightarrow Ry / \pi \rightarrow Ry$	6.83	$n_O \rightarrow Ry$	6.89 (0.03)
$n_O \rightarrow Ry / \pi \rightarrow Ry$	6.83 (.01)	$n_O (H) \rightarrow Ry$	6.91
$n_O \rightarrow Ry$	6.84 (.01)	$n_O \rightarrow Ry$	6.94
$n_O \rightarrow Ry$	6.86 (.03)	$n_O \rightarrow Ry$	6.97 (0.04)
$\pi \rightarrow Ry$	6.87 (.01)	$\pi \rightarrow \pi^*$	7.00 (0.31)
$n_O (H-2) \rightarrow Ry$	6.88	$n_O \rightarrow Ry$	7.00 (0.01)
$n_O \rightarrow Ry$	6.89 (.02)	$n_O \rightarrow Ry$	7.02
$n_O \rightarrow Ry$	6.90 (.02)	$n_O (H) \rightarrow Ry / \pi^*$	7.03
$\pi \rightarrow Ry$	6.91 (.04)	$\pi \rightarrow \pi^* / \pi \rightarrow Ry$	7.04 (0.37)
$n_O (H-2) \rightarrow Ry$	6.92	$n_O \rightarrow Ry / \pi \rightarrow \pi^*$	7.04 (0.11)
$\pi \rightarrow Ry$	6.92 (.02)	$n_O (H) \rightarrow Ry / n_O (H) \rightarrow \pi^*$	7.08
$n_O \rightarrow Ry$	6.93 (.01)	$n_O \rightarrow Ry$	7.10 (0.02)
$\pi \rightarrow Ry$	6.96 (.06)	$n_O (H) \rightarrow Ry / n_O (H) \rightarrow \pi^*$	7.10
$n_O \rightarrow Ry$	6.97 (.04)	$\pi \rightarrow Ry$	7.11 (0.02)
$n_O \rightarrow Ry$	6.97 (.03)	$n_O (H) \rightarrow \pi^*$	7.13
$\pi \rightarrow Ry$	6.98	$n_O \rightarrow Ry$	7.15
$\pi \rightarrow Ry / \pi \rightarrow \pi^*$	7.00 (.14)	$n_O \rightarrow Ry$	7.17
$n_O \rightarrow Ry$	7.00	$n_O \rightarrow Ry$	7.18
$n_O (H-2) \rightarrow Ry / \pi \rightarrow \pi^*$	7.01 (.12)	$\pi \rightarrow Ry$	7.20 (0.03)
$n_O (H-2) \rightarrow Ry / \pi \rightarrow \pi^*$	7.01 (.16)	$n_O \rightarrow Ry$	7.21 (0.03)
$\pi \rightarrow Ry / \pi \rightarrow \pi^*$	7.02 (.16)		
VIE	8.40 (C-DFTB)	VIE	9.80 (C-DFTB)

Table 7 Analysis of the TD-DFT lowest energy transitions for Geo_{IED-48} (up to the 48th excited state) and Geo_{IEI-49} (up to the 46th excited state). H letter stands for HOMO orbital.

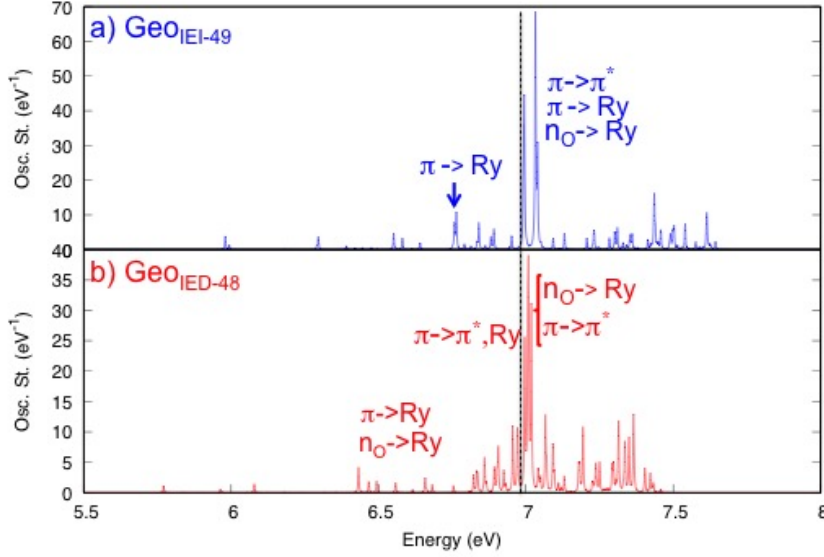


Fig. 14 TD-DFT electronic spectra (100 states) of Geo_{IED-48} (bottom red) and Geo_{IEI-49} (top blue).

4 Discussion

Our results show that for the smallest clusters, a low energy charge-transfer $Bz^+-(H_2O)_n^-$ with a non negligible oscillator strength is found at less than 7.0 eV when the oxygen of a water molecule points towards an H atom of the benzene molecule. The orbitals receiving the electron is an orbital which has a Rydberg character but which is also developed on diffuse orbitals of the atoms, in particular those of the H atoms of some water molecules. Their nature is then different from the $\pi\sigma^*$ CT states evoked by Noble et al. to account for the photoreactivity of coronene:water clusters [25] as no antibonding contribution has been observed in the populated orbitals of the excited states. The correlation between the relative orientation of the water molecule and the existence of a $Bz^+-(H_2O)_n^-$ CT state, that was clearly found when the oxygen of a water molecule interacts with an H atom of Bz, is consistent with the previous results based on experimental and theoretical synergetic studies [58]. Indeed, these studies show that, in an argon matrix, the most stable structures

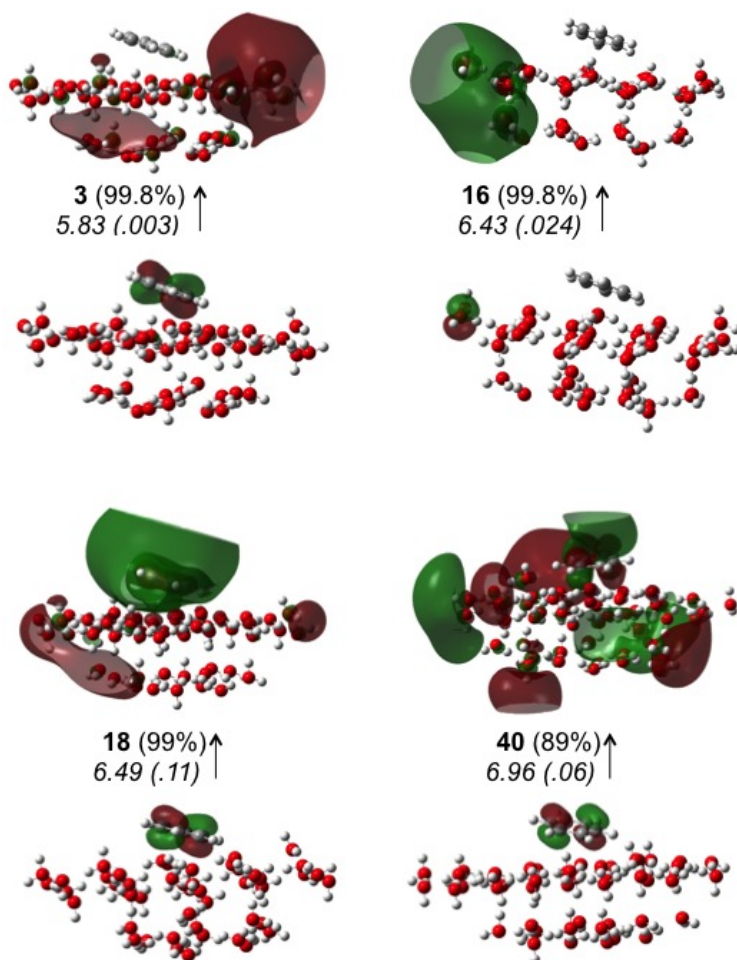


Fig. 15 Examples of NTOs involved in transitions from π and n_O orbitals to Rydberg orbitals for *GeoIED-48*. The contours' isovalues are .05 for all HOMOs and .008 for all the LUMOs (except for transition 3 for which it is .01 for the LUMO). The number of the transition, the contribution of the transition described by the NTOs with respect to the complete excited state (in %) are also reported. The energy of the transition (in eV) and oscillator strength are reminded in italics, the latter being in parenthesis.

for clusters of coronene in interaction with water monomer and dimer correspond to structures with one water molecule interacting through its oxygen atom with an H atom of the PAH within the plane of the PAH. Therefore such structures, that are not the most stable in the gas phase, would be the reactive species in the argon matrix experiments, leading to the photoactivated oxydation of the PAHs up to the formation of quinones [16,17].

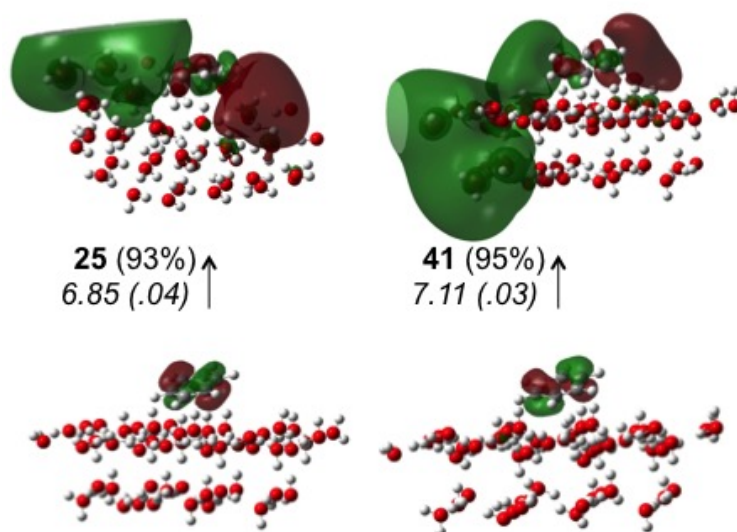


Fig. 16 Examples of NTOs involved in transitions from π to Rydberg orbitals for *GeoIEI-49*. The contours' isovalues are .05 for the HOMOs and .008 for the LUMOs. The number of the transition, the contribution of the transition described by the NTOs with respect to the complete excited state (in %) are also reported. The energy of the transition (in eV) and oscillator strength are reminded in *italics*, the latter being in parenthesis. A more complete set for the NTOs of *GeoIEI-49* are reported in the SI (*Geo_IEI_49.pdf* file).

When the size of the cluster increases, the Rydberg orbitals expand and also contain diffuse orbitals located on the H atoms of water molecules at the edge of the water clusters. Longer range transitions are involved, which can be seen on the D_{CT} distributions. Interestingly, not many ghost states were clearly found. Their nature is often ambiguous as the energy of the excited states is in the vast majority of the cases less than 1.5 eV below the M_{AC} index. We may note that the significance of such a criterion was shown for large delocalized π systems [48] and it is the first time that it is used for such molecular clusters so the conclusions concerning the ghosts states must be regarded with caution.

Overall, CT states of non negligible oscillator strength can be found below 7 eV ie less than 2 eV below the IP of isolated Bz when the latter interacts with water clusters. When these water clusters are small, our results show that such states are present when a water monomer interacts with the H atoms of Bz via its O atom. Interestingly, such conformations also tend to lead to a lowering of the IE of Bz. When the size of the cluster increases, it seems that such states are present for any configurations, including those leading to an increase of the IE of Bz.

However, we might wonder about the lifetime of such states and about their reactivity. In this respect, radical processes were also invoked for the reactivity of PAH with water, [48] which goes beyond the study presented in this work.

Finally, we may wonder whether the results obtained in the present paper for finite size systems can be applied to Bz adsorbed on water ice or embedded in water ice. Considering the larger water clusters, we showed that the electron transferred to the cluster within the CT states was located on the H atoms at the edge of the cluster. If we extrapolate our results to the Bz adsorbed on/embedded in water ice, that could mean that the transferred electron is located on the H atoms pertaining to dangling OH (dOH) bonds that could be present either in some cavities where Bz could be trapped in or on the ice surface where Bz could be adsorbed on. Indeed, recent synergetic experimental and theoretical studies based on the dOH infrared diagnosis showed that the location of Bz in ice was not clear and that it depended on the Bz:water relative concentration [33]. Interestingly, the fate of the electron determined with our approach appears quite in line with the current models, however still debated, used to describe the solvated electron. Indeed, it seems that the majority of such models are consistent with a cavity picture in which the excess electron density is self-trapped, localized and primarily contained in a solvent-free void within the water [59], which could correspond to the dOH at the surface or inside some cavities (defaults) of interstellar water ice.

5 Conclusion

In this work, we presented vertical electronic spectra and detailed analysis of the lowest energy (up to the 50th or 100th) electronic states of a Bz molecule in interaction with water clusters within different organizations and different sizes. These were extracted from two benzene-Ih ice configurations leading to maximum ionization energy on the one hand and to the minimum ionization energy of the solvated benzene on the other hand. For all systems, the electronic spectra are computed at the TD-DFT level in conjunction with an appropriate basis set containing diffuse and polarisation orbitals on the atoms and describing the Rydberg states of benzene. The approach was carefully benchmarked against MS-CASPT2 results for the smallest systems (up to 6 water molecules).

Transitions from the non bonding n_O orbitals are described at the TD-DFT level, which is not the case of MS-CASPT2 spectra due to the restricted active space. TD-DFT transitions are extremely multireferential, and one transition may involve both n_O and π orbitals as well as both Rydberg and π^* virtual orbitals. Although there are some discrepancies, the trends were found to be similar at both MS-CASPT2 and TD-DFT levels : the positions and intensities of the main $\pi \rightarrow \pi^*$ transitions hardly affected, only splitting due to symmetry

breaking was observed. The larger the systems, the more other transitions of weak oscillator strength at both lower and higher energy than these intense transitions were found, a larger number of these being transitions for n_O and n_O/π orbitals to Rydberg orbitals.

For the smallest systems, our results clearly demonstrate the influence of the clusters' structures on the spectra. In particular, only for the series of *Geo*_{IED} clusters we found a $\pi \rightarrow \text{Ry}$ (H) transition of non negligible intensity that describes the promotion of one electron to a Rydberg orbital that has an important contribution on the water molecule whose oxygen points towards the H atom of benzene. When the size increases, one can find a $\pi \rightarrow \text{Ry}$ (H) lower than 7 eV for all configurations. The difference with the small systems is that the Rydberg orbitals become mainly developed on the H atoms of the water molecules at the edge of the cluster to the detriment of the water molecules at the vicinity of the benzene molecule. These transition energies of such $\pi \rightarrow \text{Ry}$ (H) states are more than 2 eV below the IP of benzene, and can be regarded as CT states. So such states could be formed irradiating the systems under low energy photons as achieved in the photoreactivity experiments [16, 17]. However, in order to rationalize the experimental results ie the formation of a long lived CT state and its reactivity, further investigations such as non adiabatic dynamics are necessary.

6 Supplementary Information (SI)

A folder named **SI_Bz_water_TCA** contains 9 files described hereafter :

- **SI_bench_Bz_water.pdf** contains all the SI referring to the benchmark of the electronic spectrum the benzene molecule and of the water clusters as well as Rydberg basis sets generated for MS-CASPT2 calculations.
- the 8 other files named **Geo_IEI-1.pdf**, **Geo_IED-1.pdf**, **Geo_IEI-6.pdf**, **Geo_IED-5.pdf**, **Geo_IEI-12.pdf**, **Geo_IED-14.pdf**, **Geo_IEI-49.pdf** and **Geo_IED-48.pdf** contain the geometry (in xyz), the basis set, the TD-DFT energies and excitations' detailed assignments, the shape of the MOs, a list of the transitions with the corresponding D_{CT} and M_{AC} indexes. The few of the two latter values which were computed using the relaxed densities are also reported. In the case of **Geo_IEI-49.pdf** and **Geo_IEI-12.pdf**, several NTOs are also shown.

7 Acknowledgments

The authors would like to thank J. Mascetti, C. Toubin and J. Noble for fruitful scientific discussions. The authors are also deeply grateful to F. Spiegelman for his dedication to Science and his tremendous scientific expertise he has always

been eager to share with them. A.S. also acknowledges the computing facility CALMIP for generous allocation of computing resources (project P17002) at University of Toulouse (UT 3). This work has been funded by the French Agence Nationale de la Recherche, ANR PARCS project (ANR-13-BS08-0005), with support of the French research network EMIE (Edifices Moléculaires Isolés et Environnés, GDR 3533 du CNRS, the French National Program Physique et Chimie du Milieu Interstellaire (PCMI) of the CNRS/INSU with the INC/INP, co-funded by the CEA and the CNES.

References

1. E. Michoulier, N. Ben Amor, M. Rapacioli, J.A. Noble, J. Mascetti, C. Toubin, A. Simon, *Phys. Chem. Chem. Phys.* **20**(17), 11941 (2018). DOI 10.1039/C8CP01175C
2. E. Dartois, *J. Carb. Res.* **5**(4), 80 (2019). DOI 10.3390/c5040080
3. L.J. Allamandola, A.G.G.M. Tielens, J.R. Barker, *Astrophys. J.* **290**(1), L25 (1985). DOI 10.1086/184435
4. A. Léger, J.L. Puget, *Astron. Astrophys.* **137**, L5 (1984)
5. B.T. Draine, *Annu. Rev. Astron. Astrophys.* **41**, 241 (2003)
6. C. Joblin, A. Léger, P. Martin, *Astrophys. J. Lett.* **393**, L79 (1992)
7. C. Joblin, A.G.G.M. Tielens (eds.), *PAHs and the Universe: A Symposium to Celebrate the 25th Anniversary of the PAH Hypothesis*, *EAS Publications Series*, vol. 46 (2011)
8. A. Simon, M. Rapacioli, *Chemical Modelling* (Roy. Soc. Chem., 2017), *SPR (Specialist Chemical Reports)*, vol. 14, chap. Energetic Processing of PAHs : isomerisation and dissociation, pp. 195–216
9. J. Bouwman, H.M. Cuppen, M. Steglich, L.J. Allamandola, H. Linnartz, *Astron. Astrophys.* **529**, A46 (2011). DOI 10.1051/0004-6361/201015762
10. K.I. Osberg, *Chem. Rev.* **116**(17), 9631 (2016). DOI 10.1021/acs.chemrev.5b00694
11. M.P. Bernstein, S.A. Sandford, A.L. Mattioda, L.J. Allamandola, *Astrophys. J.* **664**(2), 1264 (2007)
12. J. Bouwman, H.M. Cuppen, A. Bakker, L.J. Allamandola, H. Linnartz, *Astron. Astrophys.* **511**, A33 (2010). DOI 10.1051/0004-6361/200913291
13. J. Bouwman, D.M. Paardekooper, H.M. Cuppen, H. Linnartz, L.J. Allamandola, *Astrophys. J.* **700**(1), 56 (2009)
14. M.P. Bernstein, S.A. Sandford, L.J. Allamandola, J.S. Gillette, S.J. Clemett, R.N. Zare, *Science* **283**(5405), 1135 (1999). DOI 10.1126/science.283.5405.1135
15. M.P. Bernstein, J.P. Dworkin, S.A. Sandford, L.J. Allamandola, *Meteor. and Planet. Science* **36**(3), 351 (2001). DOI 10.1111/j.1945-5100.2001.tb01878.x
16. Z. Guennoun, C. Aupetit, J. Mascetti, *Phys. Chem. Chem. Phys.* **13**(16), 7340 (2011). DOI 10.1039/c0cp01756f
17. Z. Guennoun, C. Aupetit, J. Mascetti, *J. Phys. Chem. A* **115**(10), 1844 (2011). DOI 10.1021/jp108713n
18. A.L.F. de Barros, A.L. Mattioda, A. Ricca, G. Cruz-Diaz, L.J. Allamandola, *Astrophys. J.* **848**(2), 112 (2017)
19. M. Gudipati, L. Allamandola, *Astrophys. J.* **615**, L177 (2004). DOI 10.1086/426392
20. D. Woon, J. Park, *Astrophys. J.* **607**(1, 1), 342 (2004). DOI 10.1086/383345
21. D. Porezag, T. Frauenheim, T. Köhler, G. Seifert, R. Kaschner, *Phys. Rev. B* **51**, 12947 (1995)
22. G. Seifert, D. Porezag, T. Frauenheim, *Int. J. Quantum Chem.* **58**, 185 (1996)
23. M. Elstner, D. Porezag, G. Jungnickel, J. Elsner, M. Haugk, T. Frauenheim, S. Suhai, G. Seifert, *Phys. Rev. B* **58**(11), 7260 (1998). DOI 10.1103/PhysRevB.58.7260
24. M. Gudipati, L. Allamandola, *Astrophys. J.* **638**(1, 1), 286 (2006). DOI 10.1086/498816
25. J.A. Noble, C. Jouvet, C. Aupetit, A. Moudens, J. Mascetti, *Astron. Astrophys.* **599**, A124 (2017). DOI 10.1051/0004-6361/201629613
26. J. Finley, P. Malmqvist, B.O. Roos, L. Serrano-Andrés, *Chem. Phys. Lett.* **288**(299), 299 (1998). DOI 10.1016/S0009-2614(98)00252-8

27. D. Sharma, M.J. Paterson, *Photochem. Photobiol. Sci.* **13** (11), 1549 (2014). DOI 10.1039/C4PP00211C
28. D. Sharma, W.M.C. Sameera, S. Andersson, G. Nyman, M.J. Paterson, *Chem. Phys. Chem.* **17** (24), 4079 (2016). DOI 10.1002/cphc.201600660
29. E. Michoulier, J.A. Noble, A. Simon, J. Mascetti, C. Toubin, *Phys. Chem. Chem. Phys.* **20**(13), 8753 (2018). DOI 10.1039/C8CP00593A
30. D. Sharma, M.J. Paterson, *RSC Adv.* **5** (36), 28281 (2015). DOI 10.1039/C5RA01894C
31. A.Y. Freidzon, R.R. Valiev, A.A. Berezhnoy, *RSC Adv.* **4**, 42054 (2014). DOI 10.1039/C4RA05574H
32. G. Herzberg, *Molecular spectra and molecular structure. Vol.3: Electronic spectra and electronic structure of polyatomic molecules* (1966)
33. E. Michoulier, C. Toubin, A. Simon, J. Mascetti, C. Aupetit, J.A. Noble, *The Journal of Physical Chemistry C* **124**(5), 2994 (2020). DOI 10.1021/acs.jpcc.9b09499
34. B.O. Roos, P.R. Taylor, P.E. Siegbahn, *Chem. Phys.* **48**(2), 157 (1980). DOI 10.1016/0301-0104(80)80045-0
35. F. Aquilante, L. De Vico, N. Ferré, G. Ghigo, P. Malmqvist, P. Neogrady, T.B. Pedersen, M. Pitoňák, M. Reiher, B.O. Roos, L. Serrano-Andrés, M. Urban, V. Veryazov, R. Lindh, *J. Comput. Chem.* **31**(1), 224 (2010). DOI 10.1002/jcc.21318
36. V. Veryazov, P.O. Widmark, L. Serrano-Andrés, R. Lindh, B.O. Roos, *Int. J. Quantum Chem.* **100**(4), 626 (2004). DOI 10.1002/qua.20166
37. G. Karlström, R. Lindh, P. Malmqvist, B.O. Roos, U. Ryde, V. Veryazov, P.O. Widmark, M. Cossi, B. Schimmelpfennig, P. Neogrady, L. Seijo, *Comput. Mat. Science* **28**(2), 222 (2003). DOI 10.1016/S0927-0256(03)00109-5
38. P.O. Widmark, P. Malmqvist, B.O. Roos, *Theor. Chim. Acta* **77**(5), 291 (1990). DOI 10.1007/BF01120130
39. P. Čársky, M. Urban, *Ab Initio Calculations: Methods and Applications in Chemistry, Lecture Notes in Chemistry*, vol. 16 (Springer Berlin Heidelberg, 1980). DOI 10.1007/978-3-642-93140-6
40. K. Kaufmann, W. Baumeister, M. Jungen, *J. Phys. B: At. Mol. Opt. Phys.* **22**(14), 2223 (1989). DOI 10.1088/0953-4075/22/14/007
41. J. Lorentzon, P. Malmqvist, M. Foelscher, B.O. Roos, *Theor. Chim. Acta* **91**(1), 91 (1995). DOI 10.1007/BF01113865
42. P.A. Malmqvist, B.O. Roos, B. Schimmelpfennig, *Chem. Phys. Lett.* **357**(3), 230 (2002). DOI 10.1016/S0009-2614(02)00498-0
43. T. Yanai, D.P. Tew, N.C. Handy, *Chem. Phys. Lett.* **393**(1-3), 51 (2004). DOI 10.1016/j.cplett.2004.06.011
44. E. Bohl, B. Mignolet, J.O. Johansson, F. Remacle, E.E.B. Campbell, *Phys. Chem. Chem. Phys.* **19**(35), 24090 (2017). DOI 10.1039/C7CP03913A
45. T.M. Maier, H. Bahmann, A.V. Arbuznikov, M. Kaupp, *J. Chem. Phys.* **144**(7), 074106 (2016). DOI 10.1063/1.4941919
46. T.H. Dunning, P.J. Hay, in *Methods of Electronic Structure Theory*, ed. by H.F. Schaefer (Springer US, 1977), pp. 1–27. DOI 10.1007/978-1-4757-0887-5-1
47. T. Le Bahers, C. Adamo, I. Ciofini, *J. Chem. Theo. Comput.* **7**(8), 2498 (2011). DOI 10.1021/ct200308m
48. M. Campetella, F. Maschietto, M.J. Frisch, G. Scalmani, I. Ciofini, C. Adamo, *J. Comput. Chem.* **38**(25), 2151 (2017). DOI 10.1002/jcc.24862
49. F. Maschietto, M. Campetella, M.J. Frisch, G. Scalmani, C. Adamo, I. Ciofini, *J. Comput. Chem.* **39**(12), 735 (2018). DOI 10.1002/jcc.25144
50. R.L. Martin, *J. Chem. Phys.* **118**(11), 4775 (2003). DOI 10.1063/1.1558471
51. M.J. Frisch, G.W. Trucks, H.B. Schlegel, G.E. Scuseria, M.A. Robb, J.R. Cheeseman, G. Scalmani, V. Barone, G.A. Petersson, H. Nakatsuji, X. Li, M. Caricato, A.V. Marenich, J. Bloino, B.G. Janesko, R. Gomperts, B. Mennucci, H.P. Hratchian, J.V. Ortiz, A.F. Izmaylov, J.L. Sonnenberg, D. Williams-Young, F. Ding, F. Lipparini, F. Egidi, J. Goings, B. Peng, A. Petrone, T. Henderson, D. Ranasinghe, V.G. Zakrzewski, J. Gao, N. Rega, G. Zheng, W. Liang, M. Hada, M. Ehara, K. Toyota, R. Fukuda, J. Hasegawa, M. Ishida, T. Nakajima, Y. Honda, O. Kitao, H. Nakai, T. Vreven, K. Throssell, J.A. Montgomery, Jr., J.E. Peralta, F. Ogliaro, M.J. Bearpark, J.J. Heyd, E.N. Brothers, K.N. Kudin, V.N. Staroverov, T.A. Keith, R. Kobayashi, J. Normand, K. Raghavachari,

- A.P. Rendell, J.C. Burant, S.S. Iyengar, J. Tomasi, M. Cossi, J.M. Millam, M. Klene, C. Adamo, R. Cammi, J.W. Ochterski, R.L. Martin, K. Morokuma, O. Farkas, J.B. Foresman, D.J. Fox. Gaussian16 Revision B01 (2016) Gaussian Inc. Wallingford CT
52. E. Pantos, J. Philis, A. Bolovinos, *J. Mol. Spectro.* **72**(1), 36 (1978). DOI 10.1016/0022-2852(78)90041-3
53. N. Nakashima, H. Inoue, M. Sumitani, K. Yoshihara, *J. Chem. Phys.* **73**(12), 5976 (1980). DOI 10.1063/1.440131
54. R.L. Whetten, S.G. Grubb, C.E. Otis, A.C. Albrecht, E.R. Grant, *J. Chem. Phys.* **82**(3), 1115 (1985). DOI 10.1063/1.448484
55. P. Johnson, G. Korenowski, *Chem. Phys. Lett.* **97**(1), 53 (1983). DOI 10.1016/0009-2614(83)87182-6
56. S.G. Grubb, C.E. Otis, R.L. Whetten, E.R. Grant, A.C. Albrecht, *J. Chem. Phys.* **82**(3), 1135 (1985). DOI 10.1063/1.448485
57. A. Hiraya, K. Shobatake, *J. Chem. Phys.* **94**(12), 7700 (1991). DOI 10.1063/1.460155
58. A. Simon, J.A. Noble, G. Rouaut, A. Moudens, C. Aupetit, C. Iftner, J. Mascetti, *Phys. Chem. Chem. Phys.* **19**(12), 8516 (2017). DOI 10.1039/C6CP08559H
59. L. Turi, P.J. Rossky, *Chem Rev.* **112**(11), 5641 (2012). DOI 10.1021/cr300144z